Neural coding of choice and outcome are modulated by uncertainty in orbitofrontal but not secondary motor cortex

Juan Luis Romero-Sosa[1], Alex Yeghikian[1], Andrew M. Wikenheiser[1-3], Hugh T. Blair[1-3#] & Alicia Izquierdo[1-4#]

[1]Department of Psychology, University of California-Los Angeles, Los Angeles, California, USA.

[2]The Brain Research Institute, University of California-Los Angeles, Los Angeles, California, USA.

[3]Integrative Center for Learning and Memory, University of California-Los Angeles, Los Angeles, California, USA.

[4]Integrative Center for Addictions, University of California-Los Angeles, Los Angeles, California, USA.

Author contributions:

AI: Conceptualization, methodology, formal analysis, resources, writing-original draft, writing-review & editing, supervision, and funding. **JLRS**: Conceptualization, methodology, formal analysis, investigation, data curation, writing- original draft, writing- review & editing, software, and visualization. **AY:** Investigation, data curation, formal analysis, and visualization. **AMW:** Formal analysis and writing- review & editing. **HTB:** Formal analysis, resources, writing- review & editing, supervision, and funding.

Corresponding authors:

Juan Luis Romero-Sosa and Dr. Alicia Izquierdo

Abstract

Orbitofrontal cortex (OFC) and secondary motor cortex (M2) are both implicated in flexible reward learning but the conditions that differentially recruit these regions are not fully understood. We imaged calcium activity from single neurons in OFC or M2 during *de novo* learning of increasingly uncertain reward probability schedules. Predictions of choice were decoded from M2 neurons with high accuracy under all certainty conditions, but were more accurately decoded from OFC neurons under greater uncertainty. The number of choice- and reward-selective neurons was significantly higher in M2 than in OFC across schedules, but these proportions increased across levels of uncertainty only in OFC. Decoding accuracy of choice and outcome was predicted by behavioral strategies Win-Stay and Lose-Shift in OFC, but not M2. We also tested causal involvement of these regions with chemogenetic perturbation as rats learned increasing and then decreasing uncertainty schedules. Whereas inhibition of OFC neurons attenuated learning across all schedules, M2 neurons were found to support learning in the most certain reward schedule. Thus, OFC neurons preferentially encode choices and outcomes that foster a greater reliance on adaptive strategies under uncertainty. This reveals a novel functional heterogeneity within frontal cortex in support of flexible learning.

INTRODUCTION

Both the orbitofrontal cortex (OFC) and secondary motor cortex (M2) are involved in flexible reward learning and reward-motivated decision making. M2 receives dense inputs from diverse cortices, including sensorimotor, visual, retrosplenial, and orbital regions[1], and in turn, sends projections to striatum that fall along mediolateral and rostrocaudal gradients within M2[2], enabling precise control of actions. This anatomical connectivity positions M2 well to control action flexibly based on both sensory and motivation information. Functional studies have determined that M2 is essential for action updates [3] and that it enables the flexible assignment of either stimuli or motor antecedents to action plans[4-6]. Additionally, there has been discovery of different population dynamics in M2 depending on the strategy and stimulus modality that mice use in a flexible decision-making task[7]. Given its integration of sensory and motivation evidence, M2 has an essential role in higher-order movement control and orienting[8] but can also bias choice based on outcomes and choice history[9, 10]. Though a previous electrophysiological study indicated orbitofrontal cortex (OFC) is involved in updating outcome value from prior actions[11], authors found that M2 signaled choice earlier than any other area of rat frontal cortex, and remarkably also contained a value signal[12].

OFC also has a well-substantiated role in flexible decision making[13-16]. Several groups have reported choice-predictive neurons in OFC in equivalent or even larger numbers than value or outcome-encoding cells in this region[17-21]. One group found that over half of the neurons they recorded in OFC encoded both the direction of choice and the location of the goal, concluding that choice selective neurons in OFC represent spatial-motor information required to define specific goals and necessary actions to obtain them[21]. However, it is presently unclear if and how these representations change with uncertainty. By uncertainty we mean stochasticity, or moment-to-moment probabilistic outcomes[22] generating an 'expected uncertainty'[23-25], not uncertainty resulting from volatility, or the rate of change[22]. Indeed, a somewhat parallel literature suggests OFC may be critically involved in learning, especially under uncertain or probabilistic conditions[26-28], where it may set the expectation for the rest of learning[24, 25, 29, 30]. This is consistent with the idea that OFC stores long-term action values[24, 31], stimulus values[32], and causally contributes to an expected uncertainty or baseline risk in rats[33, 34]. This risk is signaled by single neurons in OFC in rats [35, 36] and in nonhuman primates[37, 38]. One study[39] reported that OFC neurons track expectations across a slow timescale (i.e., across-session probabilistic reversal learning) and are also recruited for trial-by-trial learning, or value updates, on a fast timescale (i.e., within a session). However, this study did not manipulate the reward uncertainty over time. Critically, aside from the

Hattori et al. (2023) study, recording and imaging studies in both rodent and primate species typically assess the role of OFC in decisions in expert animals, not during the learning of risk or expected uncertainty. Thus, it is unknown how choice and outcome cell selectivity may change over the course of learning, especially with increasing uncertainty in OFC. All of the above suggests that although M2 and OFC are involved in flexible learning and decision-making, their involvement could dissociate over different timescales and increasingly uncertain conditions.

Using miniscopes, we compared populations of neurons and single cells in OFC and M2 over several sessions of learning in freely-behaving rats. Unlike the great number of studies assessing these regions in well-trained animals, here we studied calcium dynamics during *de novo* learning. We were primarily interested in determining if and when neural dynamics would differentially predict choice and outcome in M2 vs. OFC, and which behavioral and task features single cells were selective for in these regions across learning under uncertainty.

RESULTS

Learning under increasing uncertainty

Male and female Long–Evans rats first underwent stereotaxic surgery to infuse GCaMP6f into either M2 or OFC (see Methods). In the same surgery, a GRIN lens was unilaterally implanted over the site of the viral infusion (**Figure 1I-K**; photomicrographs of lens implant and calcium indicator expression for all rats are shown in **Supplementary Figure 1**). Following surgical recovery and baseplating, rats then underwent pretraining followed by six sessions of learning. In a touchscreen-outfitted chamber, rats were required to initiate each trial by touching a center stimulus and then make a choice to touch a stimulus on either the left or right side. If correct, rats could retrieve a sucrose pellet reward from a food port located on the opposite side of the touchscreen response zone, signaled by a light cue in the port. This visual cue appeared concurrently with pellet delivery on rewarded, but not unrewarded, trials. The reward contingencies reversed every 75 trials and increased in uncertainty on the last block of trials, with reward schedules progressing from less to more reward uncertainty (100:0 to 70:30) (**Figure 1A-B**). The probability of reward delivery depended on the rat's choice (left vs. right), with one side delivering a higher probability of reward than the other. Each session consisted of 3 blocks of 75 trials (225 trials total); the response with the highest reward probability (left vs. right) was reversed at the start of each block. Within each session, the probability ratio remained the same for the first two trial blocks and then changed to a ratio with higher uncertainty for the last block of trials. As shown in **Figure 1C**, sessions 1 and 2 used a ratio of 100:0 for blocks 1-2 and 90:10 for block 3

(Schedule 1), sessions 3 and 4 used a ratio of 90:10 for blocks 1-2 and 80:20 for block 3 (Schedule 2), and sessions 5 and 6 used a ratio of 80:20 for blocks 1-2 and 70:30 for block 3 (Schedule 3). **Figure 1D** shows an example of a single rat's performance during a Schedule 2 session.

Results of an omnibus Generalized Linear Model (GLM) with a binomial distribution on predictors of raw choices (0, 1) are found in **Table 1**. The main dependent variable was whether the rats chose the higher reward probability location. Rats improved on this measure across trials (GLM: $\beta_{trialnum}$ = 0.0559, $p < 0.001$) and blocks (β_{block} = 1.6671, $p < 0.001$), but not across

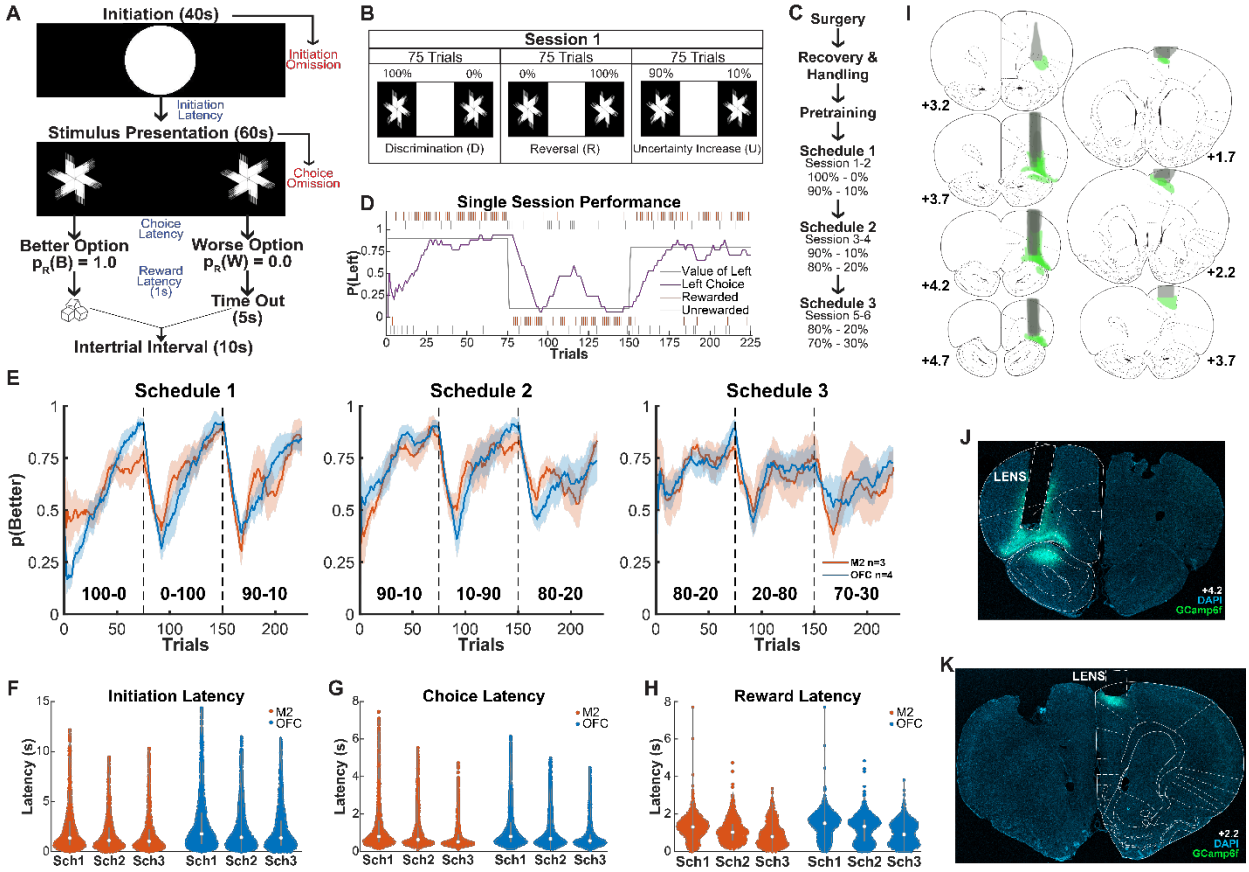

Figure 1. Probabilistic reversal learning task performance in freely-behaving, lens-implanted rats. **(A)** Schematic of trial timeline: Rats learn in an operant chamber outfitted with a touchscreen with three different interaction zones (left, center, and right) and a reward port on the opposite side of the chamber. A white circle is presented in the middle zone for 40 seconds, during which the rat is required to nosepoke to initiate a trial. Subsequently, two identical stimuli are presented on the left and right side of the screen for 60 seconds. The rat is required to nosepoke one of these stimuli, selecting either the left or right side. One of the sides has a higher reward probability than the other. The rat either gets rewarded 1 s after the nosepoke or undergoes a 5-second timeout. There is a 10 second Intertrial Interval (ITI) before a new trial begins. **(B)** A session consists of 3 blocks of 75 trials each, with two reversals, with the last block increasing in uncertainty. **(C)** Following surgery, recovery, handling, and pretraining to respond to touchscreen stimuli on either the left or the right, different schedules are introduced, with each schedule administered across two days each, and increasing in uncertainty. **(D)** Sample performance on Schedule 2 where the rat matches the value of the left side and adapts its behavior following a reversal. **(E)** There was a significant difference in accuracy, p(Better), by lens implant area (**Table 1**). **(F-H)** Performance measures by lens implant region to include latencies for Initiation **(F)**, Choice **(G)**, and Reward **(H)** for M2- and OFC-lens implanted rats across all the schedules. **(I)** Reconstructions of calcium indicator GCaMP6f and GRIN lens implant in all rats. **(J)** Photomicrograph of a lens in OFC. **(K)** Photomicrograph of a lens in M2.

schedules ($\beta_{schedule}$ = 0.1454, p = 0.58), **Figure 1E**. The M2 lens-implanted group exhibited attenuated learning compared to the OFC lens-implanted group (β_{area} = 1.6671, p = 0.0416) (**Table 1**).

Implanted animals also exhibited slightly attenuated learning compared to viral, non-tethered controls (GLM: $\beta_{Implanted_Lens}$ = -0.18, $p < 0.01$, **Supplementary Figure 2, Supplementary Table 1**). For latency measures, non-tethered control animals initiated trials and collected rewards more quickly but exhibited slower choice latencies (**Supplementary Tables 2-4**). Latencies to initiate trials and collect reward did not differ in M2- vs. OFC-implanted animals, but choice latencies were faster in the OFC-implanted animals than in the M2-implanted animals (GLM: β_{Area} = -0.57, $p < 0.01$, **Figure 1F-H**, **Tables 2-4**).

Decoding choice from calcium activity

Binary support vector machine (SVM) classifiers were trained to predict *Chosen Side* (left vs. right) from calcium traces aligned to the choice nosepoke (**Figure 2A-B)**. To determine the most appropriate windows for statistical analysis, we generated peak-aligned heatmaps and found cells that exhibited time-locked activity to either choice or reward cue **(Figure 2D-E)**. Decoder training sets were balanced to include an equal number of rewarded/unrewarded and left/right trials across all schedules (**Figure 2C**). In both M2 and OFC, choice decoding accuracy ramped up from chance starting prior to trial initiation (suggesting that rats often anticipated which side they would choose prior to trial initiation), and peaked ~500 ms after choice (**Figure 2F**). An analysis of predictors of decoding accuracy in the bin just prior to choice (yellow shaded region in **Figure 2F**) resulted in more accurate decoding in M2 than OFC (β_{Area} = -0.231, p = 0.0004), with no effect of schedule ($\beta_{Schedule}$ = -0.0843, p = 0.19), but a significant Area x Schedule interaction ($\beta_{Area:Schedule}$ = 0.056, p = 0.0475), **Table 5**. *Chosen Side* was decoded from M2 with similarly high accuracy under all probability schedules, whereas decoding was more accurate in OFC when the schedule was more uncertain. Confirming this, post-hoc analyses on each schedule (**Table 6**) revealed that decoding from M2 was more accurate than from OFC under conditions of higher certainty (Schedule 1: β_{Area} = -0.174, p = 0.0027; Schedule 2: β_{Area} = -0.119, p = 0.0438), but under the least certain schedule, OFC decoding accuracy increased to become equivalent to M2 decoding accuracy (Schedule 3: β_{Area} = -0.0621, p = 0.073). This certainty-dependent decoding accuracy in OFC was not accounted for by experience (i.e., session) since experience was a covariate in the GLM model and was not a significant predictor of choice accuracy ($\beta_{Session}$ = 0.0268, p = 0.234). Additionally, to check if the number of neurons used to train decoders affected decoder accuracy, we entered this variable as a moderator in the GLM. We did not find any

significant effect or interaction with any other variable ($\beta_{NumCells}$ = -0.0008, p = 0.22, $\beta_{NumCells:Area}$ = 0.0008, p = 0.12, $\beta_{NumCells:schedule}$ = 0.0004, p = 0.17, $\beta_{NumCells:Area:schedule}$ = -0.0003, p = 0.19), indicating that ensemble size did not significantly explain decoder accuracy results.

Decoding outcome from calcium activity

SVM classifiers were trained to predict *Trial Outcome* (rewarded vs. unrewarded) from calcium traces aligned to the choice nosepoke (**Figure 2A-B**). At time points before the outcome was known (that is, prior to 1 second after the choice nosepoke), the accuracy of outcome

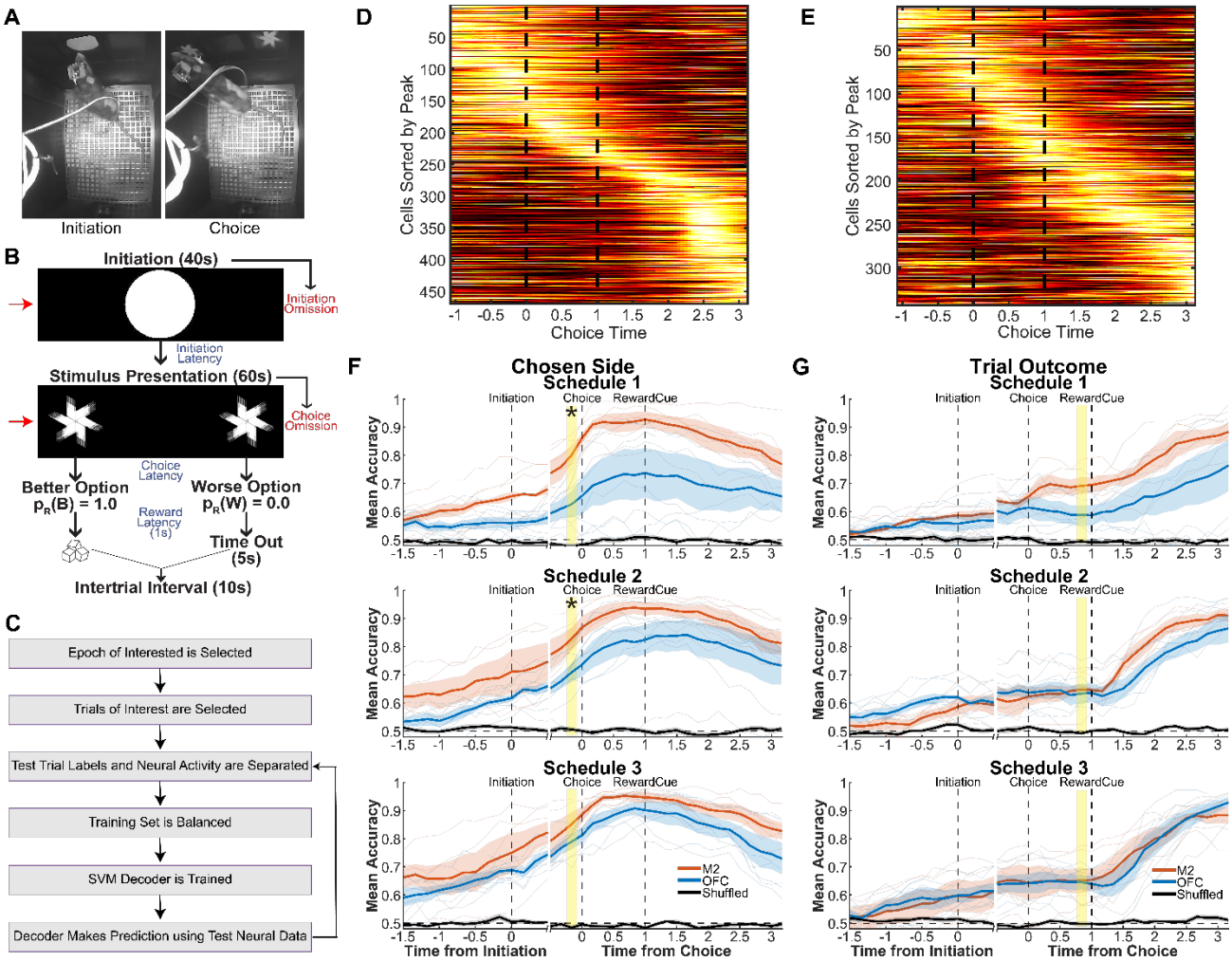

Figure 2. OFC, but not M2, choice decoding accuracy increases with uncertainty. **(A)** Trial epochs selected for analysis of neural data: Initiation (left) and Choice (right). **(B)** Same epochs in A, shown in the trial timeline. **(C)** A flowchart of how the decoder was trained with balanced data and then tested on each trial. **(D)** Example of a cross-validated peak-aligned heatmap aligned at choice from an imaging session in M2 during schedule 2. **(E)** Same as D but in OFC. **(F)** Decoder accuracy from an SVM binary decoder trained using balanced neural data from either M2 or OFC. The solid line is the mean and the shaded region is the standard deviation. The decoder was trained to predict whether the choice would be left or right (*Chosen Side*). We found a main effect of Area and Area x Schedule interaction, with post-hoc analysis revealing better decoding in M2 than OFC in Schedule 1 and 2, but not Schedule 3. Decoder accuracy using shuffled neural data in both M2 and OFC is shown in black. **(G)** Similar to F but here the decoder was trained to predict whether the trial would be rewarded or not (*Trial Outcome*). We found main effects of Area and Schedule, but no significant interaction of Area x Schedule. *p< 0.05.

decoding was limited by the certainty of the outcome (which was highest under Schedule 1 and lowest under Schedule 3). In both M2 and OFC, decoding accuracy for *Trial Outcome* began ramping up from chance at trial initiation and then stalled at a plateau which persisted until the outcome was known, after which decoding accuracy began ramping upward again (**Figure 2G**). A GLM analysis of decoding accuracy in the bin just prior to the outcome (yellow shaded region in **Figure 2G**) resulted in, as expected, better decoding of outcome for certain than uncertain schedules ($\beta_{Schedule}$ = -0.128, p = 0.0494). Decoding was also more accurate in M2 than OFC (β_{Area} = -0.138, p = 0.0248). There was similarly no effect of overall experience, or session number (**Table 7**). Here we also included the number of neurons as a moderator and again did not find a significant effect or interaction of ensemble size with any of the other predictors ($\beta_{NumCells}$ = -0.00001, p = 0.98, $\beta_{NumCells:Area}$ = 0.0002, p = 0.59, $\beta_{NumCells:schedule}$ = 0.0002, p = 0.34, $\beta_{NumCells:Area:schedule}$ = -0.0002, p = 0.31). The same analysis was conducted on only co-registered cells (i.e., the decoder was trained on session 1 and tested on session 2, within the same schedule), **Supplementary Figure 6**. This revealed a similar pattern as **Figure 2F** and pointed to greater stability for Chosen Side decoding over Trial Outcome.

The ratio of choice, outcome, and reward-selective neurons increases with uncertainty in OFC, but not in M2

To link the decoder results to single cell selectivity, we removed an increasing number of cells with large beta coefficients (**Supplementary Figure 3**). As expected, decoder accuracy steadily dropped as more neurons with the largest beta coefficients were removed. We show heatmap plots of average trial activity for neurons that were significantly selective ($p<0.05$) for *Chosen Side*, *Trial Outcome*, and *Reward Retrieval* (**Figure 3A-C**), as well as trial-by-trial raster plots of calcium activity from individual example cells (**Figure 3G-I**).

M2 contained a higher ratio of neurons selective for *Chosen Side* than OFC throughout all schedules (GLM, β_{Area} = -0.238, p < 0.01). There was a significant interaction between area and schedule (GLM, $\beta_{AreaxSchedule}$ = 0.063, p = 0.007) (**Table 8**), reflecting the fact that the ratio of choice-selective neurons increased in OFC with uncertainty (GLM, $\beta_{Schedule}$ = 0.06, p < 0.01, **Figure 3D**), but was not influenced by uncertainty in M2 (GLM, $\beta_{Schedule}$ = 0.004, p = 0.78) (**Table 9**). Session (i.e., experience) was not a significant predictor of cell selectivity. Thus, the ratio of choice-selective neurons increases in OFC with uncertainty, but does not change with uncertainty in M2.

For the *Trial Outcome* epoch, we did not find a significant region difference in the ratio of outcome-selective cells, (GLM, β_{Area} = -0.10, p = 0.068). This ratio was also not modulated by experience alone as session was not a significant predictor. We did, however, find a significant main effect of schedule (GLM, $\beta_{Schedule}$ = -0.01, p = 0.044) and a significant interaction of area and schedule (GLM, $\beta_{AreaxSchedule}$ = 0.05, p = 0.03, **Table 10**), resulting from the fact that the ratio of outcome-predictive neurons in OFC increased with increasing reward uncertainty (GLM, $\beta_{Schedule}$ = 0.03, p = 0.009; **Figure 3E**), whereas the ratio of outcome-predictive neurons in M2 was similar regardless of uncertainty (GLM, $\beta_{Schedule}$ = -0.015, p = 0.44) (**Table 11**). It is somewhat paradoxical to observe that the proportion of neurons encoding trial outcome in M2 remained stable despite decreases in the certainty of reward. One explanation for this could be that under conditions of greater uncertainty, additional M2 neurons are recruited to encode choices.

Prior evidence suggests that value integration may occur at the time of *Reward Retrieval*[29, 40-42], so we performed an additional analysis to measure the proportion of neurons that were reward-selective during a 1-s time window centered on head entry into the reward port during rewarded trials versus a corresponding time window from unrewarded trials (see Methods). There was a larger proportion of reward-selective cells in M2 compared to OFC (GLM, β_{Area} = -0.27, p = 0.02) with a significant area by schedule interaction (GLM, $\beta_{AreaXSchedule}$ = 0.1, p = 0.048) (**Table 12**), resulting from the fact that OFC exhibited a higher proportion of reward-selective neurons for schedules with greater uncertainty (GLM, $\beta_{Schedule}$ = 0.09, p = 0.032, **Figure 3F**), whereas in M2 there was a similar proportion of reward-selective neurons across all schedules (GLM, $\beta_{Schedule}$ = -0.01, p = 0.68). M2 neurons thus appear to be more heavily recruited overall to encode reward as well as choices (described above) compared to OFC neurons. Finally, it is an increase in uncertainty and not experience (**Table 13**) that drives the increase in the ratio of reward-selective cells in OFC, since session was once again not a predictor of cell selectivity.

214

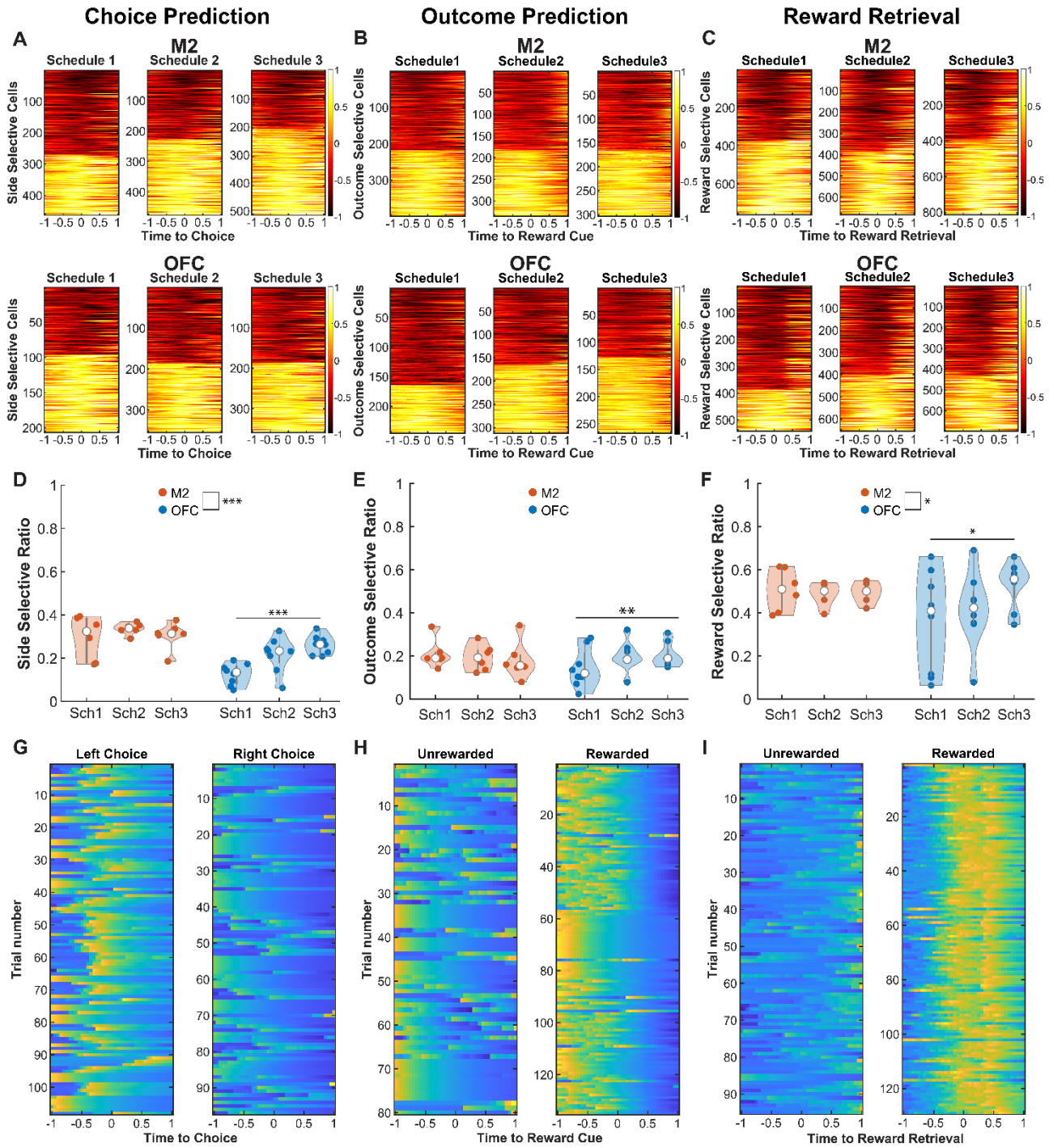

Figure 3. Decoder results are explained by changes in the ratio of selective cells across schedules. **(A)** Each row plots the difference in trial averaged activity of left trials minus right trials triggered by the time of choice. Cells plotted are all imaged neurons where we observed a significant effect of side, sorted from most negative beta coefficient to most positive one. The activity of the neurons was range-normalized. A value closer to 1 indicates more selectivity for the left side trials and a value closer to -1 indicates more selectivity for the right side. **(B,C)** Same as A but the difference is averaged activity of unrewarded trials minus rewarded trials, centered at time of reward cue (B) or reward retrieval (C). **(D)** Ratio of side selective neurons is overall larger in M2 but it increases with schedule only in OFC. **(E)** Ratio of outcome selective neurons increases with uncertainty only in OFC. **(F)** Ratio of reward selective neurons is overall larger in M2 but increases with schedule only in OFC. **(G)** Example of the z-score normalized activity of a significant side-selective M2 neuron on left and right trials. **(H)** Same as G but for a significant outcome-selective M2 cell. **(I)** Same as G but for a significant reward-selective OFC neuron. *p<0.05. ***p<0.001.

Behavioral strategies predict decoding accuracy in OFC, not in M2

To assess the degree to which different behavioral measures (**Figure 4A-F**) modulated decoding accuracy in OFC and M2, we analyzed the data using an omnibus mixed-effects GLM for *Chosen Side* (**Table 14**) and *Trial Outcome* (**Table 16**). As predictors, we included primary behavioral measures described above such as median initiation, choice, and reward latencies for the entire session (**Figure 4I-K**), as well as secondary measures such as Win-Stay (WS, proportion of trials when the rat repeated a response for which it had been rewarded on the previous trial) and Lose-Shift (LS, proportion of trials when the rat did not repeat a response for which it had been unrewarded on the previous trial), which we and others have previously used to assess adaptive strategies in both stimulus and action-based learning[24, 43]. As other predictors, we included a Flexibility Index (see Methods) that measured the animal's ability to adapt to trial block reversals, and a Perseveration Index, or the mean number of trials to shift choice behavior after being unrewarded, divided by the number of first unrewarded trials[44].

We found significant M2 vs. OFC area interaction effects for Win-Stay, Lose-Shift, and Perseveration Index in the bin just before the choice epoch (**Figure 4H**, **Table 14**). Post-hoc GLMs revealed that only initiation latencies (GLM: $\beta_{InitiationLatency} = -0.067$, $p = 0.0324$) significantly predicted *Chosen Side* decoder accuracy for M2 (**Figure 4I**, **Table 15**). In contrast, WS (GLM: $\beta_{WinStay} = 0.843$, $p = 0.0008$) and LS (GLM: $\beta_{LoseShift} = 1.466$, $p = 0.0240$) positively predicted, whereas Perseveration Index (GLM: $\beta_{Perserveration\ Index} = -4.128$, $p < 0.0001$) negatively predicted *Chosen Side* decoder accuracy in OFC (**Figure 4J**, **Table 15**). Similar post-hoc GLMs (**Figure 4K**, **Table 16**) found no significant behavioral predictors for *Trial Outcome* decoding accuracy in M2 (**Figure 4L, Table 17**), but again found that WS (GLM: $\beta_{WinStay} = 0.652$, $p = 0.0202$) and LS (GLM: $\beta_{LoseShift} = 1.550$, $p = 0.0228$) positively predicted and Perseveration Index (GLM: $\beta_{Perserveration\ Index} = -1.543$, $p = 0.0498$) negatively predicted *Trial Outcome* decoding accuracy in OFC (**Figure 4M, Table 17**). These analyses indicate that complex, strategy-level behaviors contribute to decoding accuracy in OFC, but not M2.

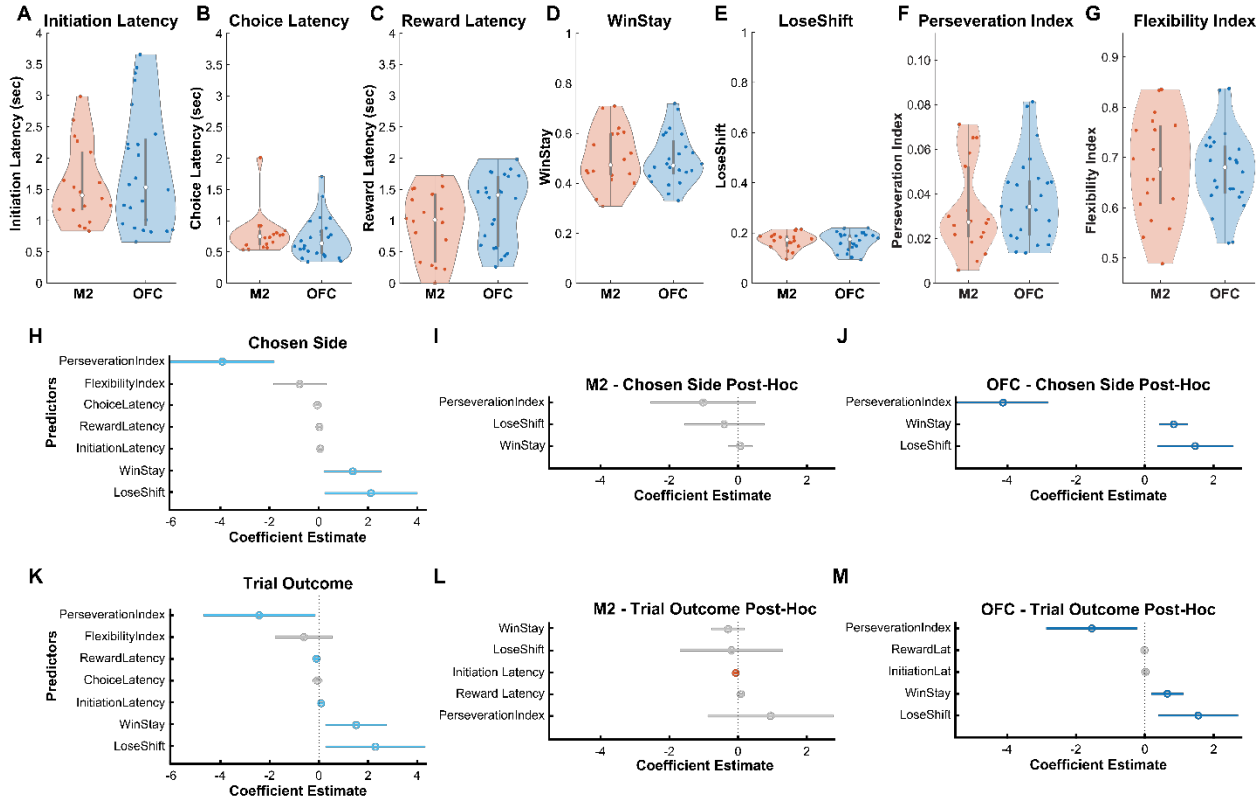

Figure 4. Chosen Side and Trial Outcome decoding accuracy is predicted by behavioral strategy only in OFC. **(A-G)** Behavioral measurements that were entered as regressors in omnibus Generalized Linear Models (GLM). Latency measures **(A-C)** were calculated as medians of all trials for each session. WinStay and LoseShift **(D-E)** were calculated as the proportion of total trials that were WinStay and LoseShift at the session level. Perserveration Index and Flexibility Index **(F-G)** were calculated using formulas described in the Methods. **(H)** Beta coefficients for regressors where significant area (M2 vs. OFC) interactions were found in predicting decoder accuracy of *Chosen Side*. Modeling was performed only on the accuracy from the bin right before choice (highlighted in yellow, Figure 2) **(I)** Post-Hoc GLM performed on sessions from rats with lenses in M2. **(J)** Post-Hoc GLM performed on sessions from rats with lenses in OFC. Strategy indices were significant predictors of *Chosen Side* decoding accuracy in OFC, but not in M2. **(K)** Beta coefficients for regressors where significant area (M2 vs. OFC) interactions were found in predicting *Trial Outcome*. Similarly, to H, analyses were only performed on the bin before reward cue (highlighted in yellow, Figure 2). **(L)** Post-Hoc GLM performed on sessions from rats with lenses in M2. **(M)** Post-Hoc GLM performed on sessions from rats with lenses in OFC. Strategy indices were significant predictors of *Trial Outcome* decoding accuracy in OFC, but not in M2.

OFC, but not M2, neurons preferentially support adaptive learning under uncertainty

Male and female Long-Evans rats underwent stereotaxic surgery to infuse hM4Di DREADDs in either OFC or M2 (see Methods). After following the same pretraining scheme as rats with lens implants, this cohort performed schedules first in order of increasing (i.e., ascending) uncertainty- identical to the cohort with lens implants- and then in order of decreasing uncertainty, which rats with lens implants did not experience. Each schedule was administered

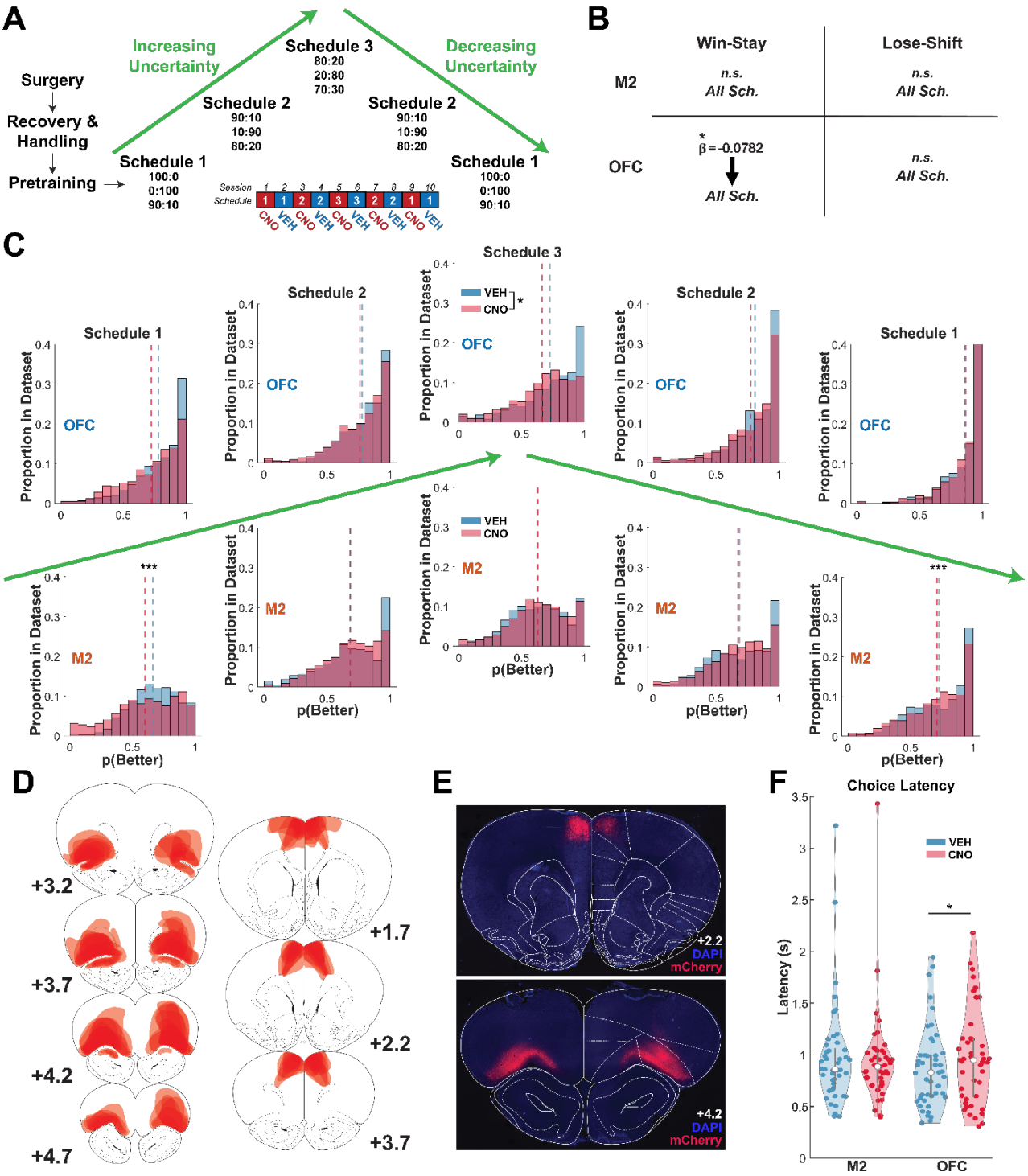

Figure 5. OFC, but not M2, neurons support learning under all uncertainty levels. **(A)** Following surgery, recovery, handling, and pretraining rats were introduced to different schedules, first in increasing order of uncertainty followed by decreasing (reverse) order. Each schedule was administered across two days, the first under CNO inhibition and the second following an injection of vehicle (VEH). **(B)** Win-stay behavior was reduced across all schedules following OFC inhibition, but not M2. **(C)** OFC inhibition resulted in attenuated accuracy throughout learning. In contrast, M2 inhibition impaired only Schedule 1 performance (CNO: β_{Drug} = -0.2018, p < 0.0001). **(D)** Reconstructions of DREADD expression across all rats. **(E)** Representative photomicrographs of hM4Di-mCherry DREADD expression in M2 and OFC. **(F)** OFC, but not M2, inhibition slowed choice latencies. *p<0.05 ***p<0.001.

twice- with CNO inhibition on the first session and an injection of vehicle (VEH) on the second

session- before the rat advanced to the next schedule (**Figure 5A**).

As in **Figure 1E**, accuracy was measured as the raw choice (0,1) of the higher reward probability option (see Methods). Using omnibus GLMs with binomial distribution (**Tables 18 and 19**), we assessed if there were interactions between schedule (1, 2, 3), order (ascending or descending uncertainty), and drug (CNO, VEH). OFC inhibition impaired accuracy across all schedules, as the effect of drug did not interact with schedule or order (CNO: $\beta_{Drug} = -0.2831$, $p < 0.02$), **Table 18**. In contrast, while there was also an effect of inhibition of M2 on accuracy (CNO: $\beta_{Drug} = -0.4698$, $p < 0.0001$), there was a drug by schedule interaction (**Table 19**), which revealed its effect was in Schedule 1 (CNO: $\beta_{Drug} = -0.2018$, $p < 0.0001$) (**Table 20**). Due to an interaction of drug by order, we conducted a post-hoc analysis which revealed that decreased performance following M2 inhibition was in the ascending (CNO: $\beta_{Drug} = -0.0950$, $p = 0.0176$) but not descending order (**Table 21**). Consistent with prior findings, OFC neurons support first reversal experience[24, 31, 45] as well as learning under all subsequent uncertainty levels. In contrast, the largest effect size for M2 neuron involvement during learning occurred in Schedule 1.

We also examined the effect of inhibition on adaptive strategies (**Tables 22–25**). OFC inhibition reduced the Win-Stay strategy across all schedules (CNO: $\beta_{Drug_CNO} = -0.020$, $p < 0.01$), with no effect on Lose-Shift. M2 inhibition had no significant effect in the use of either strategy (**Figure 5B**). Finally, we analyzed initiation, choice, and reward latencies following inhibition. While M2 inhibition had no effect on choice latencies (**Table 26**), OFC inhibition significantly slowed choice latencies (**Table 27**) (**Figure 5F**). All analyses included only animals with confirmed, bilateral expression (**Figure 5D–E**).

DISCUSSION

We imaged single-cell activity in M2 and OFC while freely-moving rats underwent learning. Using a binary support vector machine decoder, we found evidence of functional heterogeneity in frontal cortex at both the population- and single-cell level. Specifically, M2 consistently contained more information about choice on individual trials than OFC, yet decoder accuracy increased with uncertainty, not just experience, only in OFC, not M2. We found that decoder accuracy was predicted by adaptive strategies in OFC, but not M2. We also determined that M2 and OFC neurons exhibited different neural trajectories in learning trial types: these changed dynamically in more uncertain schedules in OFC, but not M2 (**Supplementary Figure 4**). Our single cell analyses revealed a recruitment of an increasing ratio of choice-, outcome- and reward- selective

neurons in OFC with uncertainty, not M2. Finally, chemogenetic inactivation of each of these regions confirmed functional roles for OFC, but not M2, as preferentially involved in learning under uncertainty. Collectively, these results suggest that neurons in OFC are more engaged in conditions with greater task demands that require adaptive strategies, such as increased uncertainty during learning.

There are several novel and confirmatory findings here. First, studies of neural activity in the frontal cortex in mice[46], rats[47, 48], and especially non-human primate subjects [49] typically involve extensive training prior to surgery to ensure that the animal is a task expert prior to any recording or imaging. In contrast, in the present experiment, rats learned the task *de novo* while we imaged single cells from these regions, which allowed us to determine that the dynamics in OFC changed as the uncertainty increased. Quite differently, M2 signaling of choice was robust and stable throughout the experiment. With the exception of two single-unit electrophysiological studies[11, 12], these two brain regions have not been systematically compared for their signaling in a reward-motivated task until now, and importantly, the previous studies administered a dynamic foraging task where subjects were not required to learn any task structure. We used a similar task to that in a recent report by Hattori and colleagues[39], but those authors also did not vary the uncertainty in the reward environment, as we did here. Consistent with their findings, we confirm that OFC plasticity is required for 'across session' learning (what authors call "meta-learning"), and here we extend this to conditions of increasing uncertainty encoded in OFC, but not in M2, neurons.

Studies following manipulations in rat OFC in flexible reward learning have included targeting the entire ventral surface [50, 51] or comparisons of medial vs. lateral OFC[27, 28]. Similar to a recent study using identical targeting[24], here we examined the role of ventrolateral OFC, a subregion not as often probed as medial and more lateral OFC[52], and found evidence consistent with its encoding of expected uncertainty[25]. Specifically, several studies using different methods [32-34, 53] suggest OFC must be 'online' to establish a baseline risk associated with probabilistic outcomes from which to gauge meaningful changes (i.e., reversals or block switches). OFC-inhibited animals also do not employ effective Win-Stay strategies[24], consistent with the GLM modeling results of the imaging experiment and the causal chemogenetic perturbation result here. A limitation in the present experimental design is that we inactivated OFC or M2 neurons on the first experience with each schedule (i.e., CNO was administered on the first and VEH was administered on the second of two sessions of each schedule). While there is converging evidence that OFC is most involved in first reversals[24, 31, 45] we were mainly interested in the pattern across schedules, and across M2 vs. OFC, not within a schedule. Indeed, we found the pattern

316 of learning attenuations was different across schedules, and the two regions supported different
317 facets of learning.

318 We also find evidence that OFC neurons learn task structure details that are ultimately
319 useful in predicting the consequences of decisions in uncertain and/or novel conditions[54]. In
320 support of this, we found that OFC neurons do not encode choices as well as M2 neurons during
321 more certain schedules, evidenced in both decoder and stability analyses where M2 decoder
322 accuracy is greater than that of OFC in the more certain schedules. Additionally, we observed an
323 increase in the proportion of neurons that signaled reward with increasing uncertainty in OFC, not
324 in M2. These findings are consistent with the idea that OFC has a pivotal role in either using or
325 creating a task map[55, 56]: just as a spatial map helps one move better through space, a task map
326 would help with adaptive behavioral strategies. We show evidence of this with decoder
327 performance in OFC positively predicted by adaptive strategies WinStay, LoseShift, and
328 negatively correlated with an inflexibility measure like Perseveration Index.

329 By comparison to OFC, M2 is often overlooked in learning studies due to its presumed
330 stronger role in motor skill and action execution in both rodents and non-human primates[57-59].
331 There is evidence that M2 encodes task-relevant features, such as whether a rat will choose the
332 left or right side in a bandit task [12] and a risky or safe option[60]. Thus, our results provide additional
333 evidence that M2 encodes important task parameters such as choice and trial outcome. Indeed,
334 M2 is relatively unchanging: its encoding of choice remained robust and dynamics in this region
335 contained a "full picture" of task-relevant features even from the initial phases of learning. In
336 support of this, we found that M2 contained information related to blocks throughout all different
337 epochs of a trial, more so than OFC **(Supplementary Figure 5)**. Additionally, chemogenetic
338 inactivation of M2 preferentially impacts learning in the most certain condition (Schedule 1). Given
339 that M2 biases decision-making processes[5, 10], a read-out of “intention” could be a useful brain-
340 machine interface application, given its stable coding.

341 These findings demonstrate distinct roles for M2 and OFC in processing task-specific
342 information during learning under uncertainty, with M2 neurons maintaining robust, stable activity
343 throughout learning, and OFC neurons exhibiting significant adaptations in response to
344 uncertainty. This suggests a mechanism by which OFC neurons make adjustments to dynamic
345 environments, while M2 provides a more consistent response control mechanism. Interestingly,
346 unlike the present findings that suggest a role for rodent OFC in both outcome and reward
347 probability encoding, primate OFC is not as important for encoding of reward “availability, as
348 indexed by its probability”[61]. Instead, OFC is more specialized in primates for value and

349 “desirability,” not probability. This may be an important primate-rodent difference to consider when
350 interpreting experimental findings in frontal cortex across species in the future.

351

352 **Acknowledgements**

353 This work was supported by NIH 2R01DA047870, NSF NeuroNex 1707408, and NIH
354 F31MH135698. We thank the members of the Izquierdo and Wikenheiser labs for their feedback
355 and suggestions. We would also like to thank Dr. Evan Hart for technical guidance and training
356 and the members of Romero Sosa’s dissertation committee, Drs. Kate Wassum and Dean
357 Buonomano, for their feedback on experimental design. Finally, we thank Dr. Dmitriy Lisitsyn for
358 help setting up the CaImAn pipeline and Dr. Alireza Soltani for his valuable feedback on
359 analyses and interpretation.

360

361 **METHODS**

362 **Subjects**

363 A total of N=32 Long-Evans rats was used. Subjects for single-cell calcium imaging were
364 n=7 adult Long-Evans rats: n=4 (3 males, 1 female) with lenses in OFC and n=3 (2 females, 1
365 male) with lenses in M2. Subjects for chemogenetic manipulation were N=25 adult Long-Evans
366 rats. Of these, seven animals were excluded from analyses: one due to a failure to complete
367 pretraining and six due to weak or unilateral viral expression. Thus, the total for the chemogenetic
368 experiment was N=18: OFC: n=9, 5 females; M2: n=9, 5 females. Rats were obtained from a
369 colony of GAD-Cre transgenic rats (RRRC#751; Rat Resource and Research Center, MO) / TH-
370 Cre (RRRC#659; Rat Resource and Research Center, MO), genotyped as wildtype. Rats were
371 pair-housed when they arrived at our housing facilities and then single-housed after undergoing
372 surgery. Rats were housed in plastic transparent tubs filled with bedding media made of wood
373 shavings in a room with a reverse 12-hour light cycle. Pretraining and testing occurred during their
374 dark period, seven days per week until all experimental sessions were completed. Motivation was
375 achieved through a progressive food restriction until the weight was kept above 85% of their initial
376 free-feeding weight. Rats had free access to water at all times. Before training, rats were handled
377 for 10-20 min for a minimum of 5 consecutive days. Subsequently, rats were introduced to a three-
378 finger hold that enabled intraperitoneal injections or the attachment of a miniscope after

379 baseplating. Experiments were conducted with the approval of, and following the guidelines
380 established by, the Chancellor's Animal Research Committee at UCLA.

381 **Behavioral Pretraining**

382 Our operant chambers were outfitted with a touchscreen on one end, divided into three
383 zones (left, center, and right), and a reward port opposing the touchscreen (Models 80604 and
384 80604A, Lafayette Instrument, Inc., Lafayette, IN). Ten sucrose pellets were placed in the rat's
385 homecage one day before training to acclimate them to the pellets. The rats were placed in the
386 operant chambers on the first training day, and 5 pellets were dispensed. The rats remained in
387 the chambers for 20 min, where they could explore, eat the pellets, and become habituated to the
388 testing environment. The criterion for the rat to move on to the next phase is eating all 5 pellets
389 within the allotted time. The following day, they begin Initial Touch Center (ITC), which was the
390 first time the rat had learned to interact with the touchscreen. A trial commenced with the display
391 of a white rectangle in the center zone to indicate the rat is required to interact with it (e.g., nose
392 poke or paw touch). Once the rat interacted with the center zone, a pellet was immediately
393 delivered to the reward port. The rat only had 40 s to interact with the center zone before the
394 rectangle disappeared, and the trial was counted as an initiation omission. If the rat successfully
395 interacted with the center zone and collected the sucrose pellet, the trial was considered a
396 committed trial. For the rat to move on from ITC, it had to complete 60 committed trials within 45
397 min. The final phase of pretraining was Immediate Reward (IR). In this phase, the rat was required
398 to initiate the trial by touching the center zone when the white rectangle is presented, and then it
399 was required to touch a stimulus presented pseudo randomly either on the left or right zone of the
400 touchscreen. The rat had 60 s to interact with this stimulus to obtain a reward. Similar to the ITC
401 criterion, for the rat to complete IR, it had to complete 60 committed trials within 45 min. After
402 completing IR, rats were considered ready for surgery.

403 **Miniscope Assembly and Imaging**

404 We purchased assembled Miniscope V4.4 kits from *Open Ephys*. The miniscope was
405 placed in a 3D-printed, custom-designed, and constructed helmet (a link to the 3D design would
406 be excellent here). The 3D-printed helmet enabled us to utilize a more resilient SMA connector
407 for rat movement. Once the miniscope was fitted inside the helmet, we ensured LED power, the
408 electrowetting lens, and the CMOS were working correctly. The tether used to connect the
409 miniscope to the operating system had a female SMA connector on one end and a male HDMI
410 connector on the opposite end. A motorized commutator from Doric Lenses (Part Number:

411 AERJ_24_HDMI+4) allowed the tether to rotate with the rat. The commutator transferred the
412 signal to the miniscope DAQ v3.3, also obtained from *Open Ephys*. The DAQ sent the signal over
413 USB to a recording computer. Additionally, the DAQ produced a TTL pulse every time the
414 miniscope recorded a frame of data. These TTL pulses were recorded in parallel with TTL pulses
415 sent by the operant chamber whenever certain behaviors within a trial were performed (i.e., trial
416 initiation, reward port entry) and were used to time lock neural data to specific epochs within trials
417 and within single sessions. These TTL pulses were recorded using a CerePlex Direct data
418 acquisition system and later used to sync the neural data. The USB signal from the miniscope
419 was recorded onto a Framework Laptop 13 (11th Gen Intel) using the Miniscope DAQ Software
420 (build v1_11). All imaging was conducted at a rate of 20 frames-per-second (fps).

421 **GCaMP and Lens Implant Surgeries**

422 Rats were anesthetized with isoflurane (5% induction, 2% maintenance in 2.5 L/min O_2)
423 and placed in a stereotaxic apparatus (Kopf Instruments, Tujunga, CA). After clearing the skull,
424 we leveled the skull by ensuring the difference in DV around bregma was not greater than 0.05
425 mm. An etchant was applied to the skull for 1 min to ensure the adhesive would adhere. After
426 cleaning the etchant, we partially drilled seven tiny holes that would be used for seven anchor
427 screws (Fine Science Tools #19010-00). Two anchor screws were placed in the very front, two
428 directly posterior from bregma, two anterior to lambda, and one contralateral to where the GRIN
429 lens would be placed. Subsequently, a 1.2 mm diameter craniotomy was drilled above the brain
430 regions of interest. For OFC placement, the coordinates were AP: +3.7mm, ML: +2.5mm, and for
431 M2 placement, the coordinates were AP: +2.0mm, ML: +0.7mm. The craniotomy was cleaned to
432 ensure that the superior sagittal sinus was intact, and then the dura was carefully removed. A
433 1□L Hamilton syringe and pump delivered GCaMP6f (AVV9-CamKII-GCaMP6f-WPRE-SV40,
434 Addgene, # 100834) through cannulae and injectors in either OFC or M2. For OFC surgeries, we
435 unilaterally infused virus into two different sites (AP: +3.7mm, ML: +2.5mm, DV: −4.2mm
436 and −4.6mm). For M2, we also infused unilaterally into two different sites (AP: +2.0mm, ML:
437 +0.7mm, DV: −1.4mm and −0.9mm). We dialed down 0.05mm more ventrally in either region to
438 create a pocket for infusions. We then injected 0.5□L of GCaMP6f per site, thus totaling 1□L of
439 virus per surgery. The syringe was placed in a Hamilton pump with a speed of 0.1□L per minute.
440 Following each infusion, 5 min elapsed before the cannula was moved. Lens implantation
441 occurred immediately after viral infusions. A 23-gauge needle was attached to the stereotaxic
442 instrument, zeroed at bregma, and then lowered to make clear a path for the lens. Next, the lens
443 was lowered to the halfway point between the DV coordinates as above using a vacuum. After

444 the GRIN (Gradient Index) lens had been placed in its location, we used viscous Loctite super
445 glue to glue the sides of the lens to the top of a dry skull, then added a layer of Metabond bone
446 cement that coats the lens, anchor screws, and the most superficial layer of the skull. After
447 allowing 5-10 min for the Metabond to dry, we poured opaque dental dement on the Metabond to
448 fully cover the anchor screws and cover the sides of (but not obscure) the GRIN lens. Before the
449 dental cement thoroughly dried, we affixed a custom 3D-printed lens cover. After drying the dental
450 cement, we applied a layer of topical antibiotic to the edge of the dental cement head cap. Animals
451 were administered carprofen (5mg/kg s.c.) and saline (1cc) prior to completion of surgery. Post-
452 operative care consisted of carprofen (5mg/kg s.c.) for five days following surgery.

453 We waited 3 to 4 weeks post-surgery to allow for GCaMP expression before attaching the
454 baseplate. We anesthetized the rat for baseplating, removed the lens protector, and cleaned the
455 top of the dental cement head cap. We attached a baseplate to a fully assembled miniscope using
456 a custom 3D holder. We lowered the miniscope and the baseplate until we could focus entirely
457 on the top of the implanted GRIN lens, searching for visible expression in the area of interest,
458 then fixing the baseplate using dental cement. GCaMP expression and lens implant
459 reconstructions are shown for OFC (**Figure 1D, left**) and for M2 (**Figure 1D, right**), along with
460 representative photomicrographs (**Figure 1E-F**)**.** All GCaMP and lens placements for all animals
461 are shown in **Supplementary Figure 1**.

462 **Viral Surgeries**

463 Craniotomies were performed similarly to the GCaMP surgeries. To express inhibitory
464 hM4Di DREADDs (Designer Receptors Exclusively Activated by Designer Drug) in cortical
465 excitatory neurons, a CaMKIIα promoter drove the hM4Di-mCherry sequence (Addgene viral prep
466 # 50477-AAV8, Watertown, MA). This construct was infused bilaterally into either OFC or M2 at
467 the same coordinates as previously described. 0.5□L was infused per site, thus totaling 1□L per
468 hemisphere and 2□L per surgery. The scalp was carefully closed using self-dissolving sutures to
469 ensure a fast and less invasive recovery.

470 Experimental testing began a minimum of three weeks after surgery to allow for receptor
471 expression. Reconstructions of DREADD expression are shown for OFC (**Figure 5D, left**) and for
472 M2 (**Figure 5D, right**), along with representative photomicrographs (**Figure 5C**)**.**

473 **Behavioral Testing**

After the baseplating surgery, rats were again put on food restriction before behavioral testing: they were eased into a restricted diet over three days to no more than 85% of their free-feeding weight. Additionally, rats were once again habituated to a gentle hold and plugging the miniscope into the baseplate. Rats were given a second round of pretraining as an acclimating imaging session using a miniscope. We ensured rats performed many trials in the IR phase (> 200 trials in 45 mins) before moving the rat onto the main behavioral task.

Learning of Probabilistic Reversals. Similar to pretraining, a trial began when a circle was displayed in the center zone of the touchscreen. The rat must interact with it by nose-poking or touching it with its paw within 40 s; otherwise, it is scored as an initiation omission. After touching the circle, two identical stimuli were presented on both the right and left touchscreen zones. The rat had to interact with either the left or the right zones. The rat had 60 s to make a choice otherwise, it was scored as a choice omission. One of the zones was associated with a higher probability of reward, while the other was associated with a lower probability of reward. If the rat received a sucrose pellet reward, it was dispensed in the reward port on the opposite side of the chamber, and the subsequent trial began after a 10-s inter-trial interval (ITI). If the rat did not receive a reward, a 5-s time-out was imposed in addition to the 10-s ITI. If the rat initiated a trial and made a choice within the allotted time, the trial was scored as a committed trial regardless of whether it was rewarded. Food motivation was assessed purely by the number of committed trials, not accuracy. In each session, there were three blocks of 75 committed trials each.

From one block to the next, the location of the highest-valued side reversed. The probability of each option itself varied by block according to schedule, with Schedule 1 including deterministic blocks (100:0, 0:100, 90:10) and Schedules 2 (90:10, 10:90, 80:20) and 3 (20:80, 80:20, 70:30) being entirely probabilistic. There was an increase in uncertainty over testing. There were two primary reasons for this design: 1) reversals (i.e., block design) keep the animals engaged and less likely to fall into a motor habit of always responding left, for example, and 2) we enhance the chance of including the same cell population during learning at one level of uncertainty (e.g., 100-0) with another (90-10), if these blocks occur in the same session. Task structure is visualized in **Figure 1A**. Violin plots for all initiation, choice, and reward latencies are shown by schedule (**Figure 1I-K**), and the median per session collapsed across all schedules for each of these groups.

Chemogenetic inhibition. In the chemogenetic cohort (n=18), inhibition of OFC or M2 was achieved with systemic administration of clozapine-N-oxide, CNO (6 mg/kg, i.p., in 95% saline, 5% DMSO; HelloBio, Princeton, NJ) 30 min prior to behavioral testing. To control for the

507 nonspecific effects of injection and handling, vehicle solution, VEH (95% saline, 5% DMSO), was
508 alternatively administered. The effects of CNO were assessed in a within-subjects design where
509 rats completed each schedule twice, first under CNO administration and second with an injection
510 of VEH. To investigate learning in changing environments while controlling for the effect of task
511 experience in navigating the task, rats first completed the schedules in increasing order of
512 uncertainty, then repeated these schedules in decreasing order **(Figure 5A).**

513 **Histology**

514 Following completion of behavioral testing, all rats were euthanized with an intraperitoneal
515 dose of sodium pentobarbital and sodium phenytoin (Euthasol® Euthanasia Solution) and
516 transcardially perfused with PBS and a 4% formalin solution. Brains were extracted, placed in 4%
517 formalin solution for at least 24 h, and subsequently left in a 30% sucrose solution for at least 24
518 h. Forty µm coronal sections were mounted onto slides and coverslipped with DAPI to visualize
519 GCaMP or hM4Di-mCherry expression. Imaging was performed using a LSM 900 confocal
520 microscope (Zeiss) and BZ-X710 florescence microscope (Keyence).

521 **Post-processing calcium imaging pipeline**

522 Miniscope recording videos were processed using custom Python code and the Python
523 version of CaImAn[62]. We concatenated videos and cropped them to focus the field of view (FOV)
524 with the neural activity. We then passed it through the motion correction algorithm in CaImAn,
525 with the central parameter *gSif_filt* set between 6 and 12 for our data. All of the motion correction
526 for our data was conducted with the piece-wise rigid motion correction Boolean setting set to true.
527 We performed the non-rigid algorithm if this algorithm did not fix the motion artifacts. Once the
528 motion correction was completed, the motion-corrected videos were passed on to the CNMF-E
529 portion of CaImAn[62]. The main parameters we used for the CNMF-E were as follows: the half size
530 of a neuron = 8; the half size of the neuron's bounding box = 16; for every session, we chose a
531 value to separate the first and most significant population of minimum peak-to-noise (PNR) ratio
532 resulting in use of a range between 7-16; for the minimum correlation value we found values
533 between 0.75 and 0.85 worked best. Every other setting was left to CaImAn default. After CNMF-
534 E, we performed a component analysis. We set the Boolean parameter *use_cnn* to true so that
535 CaImAn would use a trained convolution-neural network (CNN) model to assign a value between
536 0-1 that determined how close the components matched the appearance of soma. The algorithm
537 used three different values to determine if a component should be as accepted as a cell: Spatial
538 footprint consistency (*rval*), Signal-to-Noise ratio (*snr*), and CNN threshold value (*cnn_thr*), with

539 the minimum values for each of these set to 2.5, 0.85, and 0.85, respectively. We then visually-
540 inspected random components. Since, according to CaImAn documentation, it is not advised to
541 calculate deltaF/F when using 1P data (due to the inability to confidently calculate baseline with
542 background activity) we used the function *estimates.detrend_df_f* with the flag *detrend_only* set
543 to true to calculate fluorescence where baseline has been subtracted but has not been normalized
544 by it. Additional settings used were: quantileMin = 8, frames_window = 250, use_residuals = True.
545 Finally, we calculated the deconvolved traces of the accepted components using the CaImAn
546 function *estimates.deconvolve*. This removed any change in the fluorescence not due to the
547 dynamics of the neurons. After the detrended and deconvolved values were calculated, all of the
548 outputs were saved into a .mat file (MATLAB, MathWorks Inc., Natick, MA), for all further
549 processing. In MATLAB, we combined the output from CaImAn with TTL pulses to align activity
550 of neurons around specific epochs of behavior.

551 Some of the videos had banding artefact caused by a known issue with the USB controller
552 of the UCLA miniscope DAQ. When banding occurred, we first saved the frames in which this
553 occurred and then filled the frames with the last reliable frame before the banding. Following
554 processing with CaImAn, we replaced the data from those frames with NaNs.

555 **Data Analysis**

556 All data analyses were conducted using custom-written code in MATLAB.

557 *Learning and Performance.* The probability of choosing the better option was the primary
558 measure of interest, and secondarily Initiation Latency, Choice Latency, and Reward Latency
559 were each analyzed with a series of mixed-effects General Linear Models (GLMs) (*fitglme*
560 function; Statistics and Machine Learning Toolbox) first with omnibus analyses that included lens
561 group (M2-implanted, OFC-implanted). Follow-up GLMs were conducted pending significant
562 interactions in the omnibus models. The coding of variables for GLM were: 0=females, 1=males,
563 0=OFC-implanted, and 1=M2-implanted). Statistical significance for GLM analyses was noted as
564 p-values of less than 0.05. The variable of interest p(Better) was calculated starting with a boolean
565 vector where a 1 corresponded to a choice for the better option: 1 with the higher probability of
566 reward and a 0 for the worse option. This vector of raw choices (0, 1) was then analyzed using a
567 GLM with a binomial distribution. The Win-Stay and Lose-Shift values presented in **Figure 5D**
568 and Tables 22-25 were calculated similarly to p(Better), but for the session, not trial-by-trial. A
569 boolean vector was generated for the entire session: 1 if the trial was Win-Stay / Lose-Shift and
570 0 if it was not. These boolean vectors were then inputted into *movmean* to generate a proportion

571 of trials within this window that were Win-Stay or Lose-Shift. The following are definitions of
572 predictors: *TrialNum*: The number of trials within an entire session (from 1 to 255); *Session*:
573 Experimental day (from 1-6 in the calcium imaging and 1-10 in the DREADDs experiment); *Block*:
574 The number of blocks within a single session (from 1-3); *Area*: The brain area for calcium imaging
575 (1=M2, 0=OFC); *Schedule*: The uncertainty schedule (from 1-3). The remaining predictors are
576 defined in the Results section.

577 *Cross Validated Peak-Aligned Heatmap*. A window of detrended fluorescence 1 s before
578 and 3 s after choice was obtained for every trial in a session. This resulted in a matrix of cell-by-
579 frame-by-trial averaged across all trials for a resulting cell-by-frame matrix. This was normalized
580 using the normalize function on Matlab with the 'range' parameter. The max in a cell's activity was
581 1, and the minimum was 0 to ensure fair comparison across all cells in that session. The odd trials
582 of neurons were then peak aligned and the resulting indices were used to plot the even trials
583 using *imagesc*. Vertical dashed bars show the moment of choice and the moment of reward cue.

584 *Decoder Analysis*. A 4-s window of detrended fluorescence centered around Initiation was
585 obtained for every trial in a session. Separately, another 4-s window (1-s before and 3-s after) of
586 detrended fluorescence around choice was obtained for every trial in a session. This resulted in
587 a cell-by-frame-by-trial matrix for initiation and a separate one for choice. We temporally
588 downsampled so that activity in bin 1 was the average of frames 1-6, activity in bin 2 was the
589 average of frames 3-9, and so on. Every trial was also labeled as either a left or right choice,
590 whether rewarded or unrewarded (win or lose). One trial was left out for testing the decoder, and
591 the rest of the trials were then balanced so that there would be the same number of left-rewarded,
592 left-unrewarded, right-rewarded, and right-unrewarded conditions across all sessions in training
593 of the decoder. The balanced trials were randomly selected for every test trial to sample the entire
594 dataset of trials per session. Once the balanced subset of trials was selected, the neural data for
595 that session and the labels were inputted into the Matlab function *fitcsvm* with the
596 "KernelFunction" set to 'linear.' The decoder was then tested on the neural data for the test trial,
597 and the result was tallied as a 1 if the label matched the test label and a 0 if it was mismatched.
598 This was conducted for every single trial in a session. Additionally, we reran the decoder on all
599 trials per session, but with the trial type labels randomly shifted. This data is shown as "Shuffled"
600 in **Figure 2F-G**. Statistical comparisons and post-hocs were performed using Matlab's *fitglme*
601 function, and the formulas are included in the corresponding tables. Accuracy measures from the
602 bin (average of 5 frames) before choice were utilized for the *Chosen Side* GLMs and accuracy
603 measures before the reward cue were used for the *Trial Outcome* GLM.

604 *Single Cell Selectivity GLM*. Activity for every neuron was obtained on the same bins used
605 for the GLMs for decoder accuracy. In addition to *Chosen Side* and *Trial Outcome* activity, we
606 used the averaged activity 5 frames before and after *Reward Retrieval* for single cell selectivity
607 analysis. Statistics were conducted using Matlab's *fitglme* and the formulas for γ = neural activity
608 were γ ~ [1 + side] for Chosen Side and γ ~ [1 + rewarded + side] for both Trial Outcome and
609 Reward Retrieval. We added side as a covariate to remove the influence of side selective neurons
610 appearing as Trial Outcome or Reward Retrieval selective neurons. After a GLM was fitted for
611 every cell per session, the ratio of selective cells (ones with a p-value lower than 0.05) was
612 obtained. We then fit GLM models to the ratios across both areas and all three schedules. The
613 Beta coefficients used for **Supplementary Figure 3** were optained from the same GLMs used to
614 obtain these ratios. They are also from the same time bins as **Figure 2F-G** and the Reward
615 Retrieval timepoint described above.

616 *Behavioral measurements*. Latencies were recorded from ABET in Lafayette Instrument
617 chambers. Initiation latency measured the time from the presentation of the white circle on the
618 center touch zone until a rat interacts with the middle zone. Choice latency measured the time
619 from the presentation of both stimuli to the time the rat interacts with one of the stimuli to make a
620 choice. Reward latency measures the time from the dispensed pellet until the rat enters the reward
621 port to retrieve the pellet. WinStay was calculated as the proportion of all trials when the rat
622 received a reward on the previous trial and chose the same side for the following trial. LoseShift
623 was calculated as the proportion of all trials when the rat did not receive a reward and chose a
624 different side for the subsequent trial. The Perseveration Index was calculated as the average
625 number of trials to change choice after being unrewarded. Flexibility Index was calculated as
626 follows:

627 $$FlexIndex = mean[(mean(C_{Better}\text{Block1}, C_{Better}\text{Block2}), (mean(C_{Better}\text{Block2}, C_{Better}\text{Block3})]$$

628 where C_{Better} is equal to 1 if the animal chose the better option and 0 otherwise, with the better
629 option defined according to the reward schedule for each block. Statistical comparisons and post-
630 hocs were performed using Matlab's *fitglme* function, and the formulas are included in the
631 corresponding tables. Accuracy measures from the bin before choice were utilized for the *Chosen*
632 *Side* GLMs and accuracy measures from the bin before the reward cue were used for the *Trial*
633 *Outcome* GLM.

634

REFERENCES

1. Reep, R.L., G.S. Goodwin, and J.V. Corwin, *Topographic organization in the corticocortical connections of medial agranular cortex in rats.* J Comp Neurol, 1990. **294**(2): p. 262-80.
2. Reep, R.L. and J.V. Corwin, *Topographic organization of the striatal and thalamic connections of rat medial agranular cortex.* Brain Res, 1999. **841**(1-2): p. 43-52.
3. Gremel, C.M. and R.M. Costa, *Premotor cortex is critical for goal-directed actions.* Front Comput Neurosci, 2013. **7**: p. 110.
4. Barthas, F. and A.C. Kwan, *Secondary Motor Cortex: Where 'Sensory' Meets 'Motor' in the Rodent Frontal Cortex.* Trends Neurosci, 2017. **40**(3): p. 181-193.
5. Murakami, M., et al., *Neural antecedents of self-initiated actions in secondary motor cortex.* Nat Neurosci, 2014. **17**(11): p. 1574-82.
6. Ostlund, S.B., N.E. Winterbauer, and B.W. Balleine, *Evidence of action sequence chunking in goal-directed instrumental conditioning and its dependence on the dorsomedial prefrontal cortex.* J Neurosci, 2009. **29**(25): p. 8280-7.
7. Siniscalchi, M.J., et al., *Fast and slow transitions in frontal ensemble activity during flexible sensorimotor behavior.* Nature Neuroscience, 2016. **19**(9): p. 1234-1242.
8. Erlich, J.C., M. Bialek, and C.D. Brody, *A cortical substrate for memory-guided orienting in the rat.* Neuron, 2011. **72**(2): p. 330-43.
9. Ebbesen, C.L., et al., *More than Just a "Motor": Recent Surprises from the Frontal Cortex.* J Neurosci, 2018. **38**(44): p. 9402-9413.
10. Yang, J.H. and A.C. Kwan, *Secondary motor cortex: Broadcasting and biasing animal's decisions through long-range circuits.* Int Rev Neurobiol, 2021. **158**: p. 443-470.
11. Sul, J.H., et al., *Distinct roles of rodent orbitofrontal and medial prefrontal cortex in decision making.* Neuron, 2010. **66**(3): p. 449-60.
12. Sul, J.H., et al., *Role of rodent secondary motor cortex in value-based action selection.* Nat Neurosci, 2011. **14**(9): p. 1202-8.
13. Tsuchida, A., B.B. Doll, and L.K. Fellows, *Beyond reversal: a critical role for human orbitofrontal cortex in flexible learning from probabilistic feedback.* J Neurosci, 2010. **30**(50): p. 16868-75.
14. Gardner, M.P. and G. Schoenbaum, *The orbitofrontal cartographer.* Behavioral neuroscience, 2021. **135**(2): p. 267.
15. Rudebeck, P.H. and E.A. Murray, *The orbitofrontal oracle: cortical mechanisms for the prediction and evaluation of specific behavioral outcomes.* Neuron, 2014. **84**(6): p. 1143-56.
16. Izquierdo, A., et al., *The neural basis of reversal learning: An updated perspective.* Neuroscience, 2017. **345**: p. 12-26.
17. Zhou, J., et al., *Prospective representations in rat orbitofrontal ensembles.* Behav Neurosci, 2021. **135**(4): p. 518-527.
18. Campos, M., et al., *Orbitofrontal cortical activity during repeated free choice.* Journal of Neurophysiology, 2012. **107**(12): p. 3246-3255.
19. Kimmel, D.L., et al., *Value and choice as separable and stable representations in orbitofrontal cortex.* Nature Communications, 2020. **11**(1): p. 3466.
20. Luk, C.H. and J.D. Wallis, *Choice coding in frontal cortex during stimulus-guided or action-guided decision-making.* J Neurosci, 2013. **33**(5): p. 1864-71.
21. Feierstein, C.E., et al., *Representation of Spatial Goals in Rat Orbitofrontal Cortex.* Neuron, 2006. **51**(4): p. 495-507.
22. Piray, P. and N.D. Daw, *A model for learning based on the joint estimation of stochasticity and volatility.* Nat Commun, 2021. **12**(1): p. 6587.

681 23. Woo, J.H., et al., *Mechanisms of adjustments to different types of uncertainty in the reward*
682 *environment across mice and monkeys.* Cogn Affect Behav Neurosci, 2023. **23**(3): p. 600-619.
683 24. Aguirre, C.G., et al., *Dissociable Contributions of Basolateral Amygdala and Ventrolateral*
684 *Orbitofrontal Cortex to Flexible Learning Under Uncertainty.* J Neurosci, 2024. **44**(2).
685 25. Soltani, A. and A. Izquierdo, *Adaptive learning under expected and unexpected uncertainty.* Nat
686 Rev Neurosci, 2019. **20**(10): p. 635-644.
687 26. Dalton, G.L., et al., *Multifaceted Contributions by Different Regions of the Orbitofrontal and*
688 *Medial Prefrontal Cortex to Probabilistic Reversal Learning.* J Neurosci, 2016. **36**(6): p. 1996-2006.
689 27. Hervig, M.E., et al., *Dissociable and Paradoxical Roles of Rat Medial and Lateral Orbitofrontal*
690 *Cortex in Visual Serial Reversal Learning.* Cerebral Cortex, 2019. **30**(3): p. 1016-1029.
691 28. Verharen, J.P.H., et al., *Modulation of value-based decision making behavior by subregions of the*
692 *rat prefrontal cortex.* Psychopharmacology, 2020. **237**(5): p. 1267-1280.
693 29. Young, J.J. and M.L. Shapiro, *The orbitofrontal cortex and response selection.* Ann N Y Acad Sci,
694 2011. **1239**: p. 25-32.
695 30. Keiflin, R., et al., *The orbitofrontal cortex as part of a hierarchical neural system mediating choice*
696 *between two good options.* Journal of Neuroscience, 2013. **33**(40): p. 15989-15998.
697 31. Groman, S.M., et al., *Orbitofrontal Circuits Control Multiple Reinforcement-Learning Processes.*
698 Neuron, 2019. **103**(4): p. 734-746 e3.
699 32. Namboodiri, V.M.K., et al., *Single-cell activity tracking reveals that orbitofrontal neurons acquire*
700 *and maintain a long-term memory to guide behavioral adaptation.* Nat Neurosci, 2019. **22**(7): p.
701 1110-1121.
702 33. Jenni, N.L., G. Rutledge, and S.B. Floresco, *Distinct Medial Orbitofrontal-Striatal Circuits Support*
703 *Dissociable Component Processes of Risk/Reward Decision-Making.* J Neurosci, 2022. **42**(13): p.
704 2743-2755.
705 34. Stolyarova, A. and A. Izquierdo, *Complementary contributions of basolateral amygdala and*
706 *orbitofrontal cortex to value learning under uncertainty.* Elife, 2017. **6**.
707 35. Jo, S. and M.W. Jung, *Differential coding of uncertain reward in rat insular and orbitofrontal cortex.*
708 Sci Rep, 2016. **6**: p. 24085.
709 36. Riceberg, J.S. and M.L. Shapiro, *Orbitofrontal cortex signals expected outcomes with predictive*
710 *codes when stable contingencies promote the integration of reward history.* Journal of
711 Neuroscience, 2017. **37**(8): p. 2010-2021.
712 37. O'Neill, M. and W. Schultz, *Coding of Reward Risk by Orbitofrontal Neurons Is Mostly Distinct from*
713 *Coding of Reward Value.* Neuron, 2010. **68**(4): p. 789-800.
714 38. O'Neill, M. and W. Schultz, *Risk Prediction Error Coding in Orbitofrontal Neurons.* The Journal of
715 Neuroscience, 2013. **33**(40): p. 15810-15814.
716 39. Hattori, R., et al., *Meta-reinforcement learning via orbitofrontal cortex.* Nat Neurosci, 2023.
717 **26**(12): p. 2182-2191.
718 40. Izquierdo, A., R.K. Suda, and E.A. Murray, *Bilateral Orbital Prefrontal Cortex Lesions in Rhesus*
719 *Monkeys Disrupt Choices Guided by Both Reward Value and Reward Contingency.* The Journal of
720 Neuroscience, 2004. **24**(34): p. 7540-7548.
721 41. Ostlund, S.B. and B.W. Balleine, *Orbitofrontal Cortex Mediates Outcome Encoding in Pavlovian But*
722 *Not Instrumental Conditioning.* The Journal of Neuroscience, 2007. **27**(18): p. 4819-4825.
723 42. Schoenbaum, G., et al., *A new perspective on the role of the orbitofrontal cortex in adaptive*
724 *behaviour.* Nature Reviews Neuroscience, 2009. **10**(12): p. 885-892.
725 43. Harris, C., et al., *Unique features of stimulus-based probabilistic reversal learning.* Behav Neurosci,
726 2021. **135**(4): p. 550-570.
727 44. Brigman, J.L., et al., *Pharmacological or genetic inactivation of the serotonin transporter improves*
728 *reversal learning in mice.* Cereb Cortex, 2010. **20**(8): p. 1955-63.

45. Verharen, J.P.H., et al., *Modulation of value-based decision making behavior by subregions of the rat prefrontal cortex.* Psychopharmacology (Berl), 2020. **237**(5): p. 1267-1280.
46. Bari, B.A., et al., *Stable Representations of Decision Variables for Flexible Behavior.* Neuron, 2019. **103**(5): p. 922-933.e7.
47. Hart, E.E., M.P.H. Gardner, and G. Schoenbaum, *Anterior cingulate neurons signal neutral cue pairings during sensory preconditioning.* Current Biology, 2022. **32**(3): p. 725-732.e3.
48. Constantinople, C.M., et al., *Lateral orbitofrontal cortex promotes trial-by-trial learning of risky, but not spatial, biases.* eLife, 2019. **8**: p. e49744.
49. Padoa-Schioppa, C. and J.A. Assad, *The representation of economic value in the orbitofrontal cortex is invariant for changes of menu.* Nature Neuroscience, 2008. **11**(1): p. 95-102.
50. Izquierdo, A., *Functional Heterogeneity within Rat Orbitofrontal Cortex in Reward Learning and Decision Making.* J Neurosci, 2017. **37**(44): p. 10529-10540.
51. Izquierdo, A., et al., *Basolateral amygdala lesions facilitate reward choices after negative feedback in rats.* J Neurosci, 2013. **33**(9): p. 4105-9.
52. Zimmermann, K.S., et al., *Memory Retention Involves the Ventrolateral Orbitofrontal Cortex: Comparison with the Basolateral Amygdala.* Neuropsychopharmacology, 2018. **43**(2): p. 373-383.
53. K Namboodiri, V.M., et al., *Relative salience signaling within a thalamo-orbitofrontal circuit governs learning rate.* Current Biology, 2021. **31**(23): p. 5176-5191.e5.
54. Rudebeck, Peter H. and Elisabeth A. Murray, *The Orbitofrontal Oracle: Cortical Mechanisms for the Prediction and Evaluation of Specific Behavioral Outcomes.* Neuron, 2014. **84**(6): p. 1143-1156.
55. Wikenheiser, A.M. and G. Schoenbaum, *Over the river, through the woods: cognitive maps in the hippocampus and orbitofrontal cortex.* Nat Rev Neurosci, 2016. **17**(8): p. 513-23.
56. Costa, K.M., et al., *The role of the lateral orbitofrontal cortex in creating cognitive maps.* Nat Neurosci, 2023. **26**(1): p. 107-115.
57. Alaverdashvili, M. and I.Q. Whishaw, *Motor cortex stroke impairs individual digit movement in skilled reaching by the rat.* European Journal of Neuroscience, 2008. **28**(2): p. 311-322.
58. LAWRENCE, D.G. and H.G.J.M. KUYPERS, *THE FUNCTIONAL ORGANIZATION OF THE MOTOR SYSTEM IN THE MONKEY1: I. THE EFFECTS OF BILATERAL PYRAMIDAL LESIONS.* Brain, 1968. **91**(1): p. 1-14.
59. Whishaw, I.Q., *Loss of the innate cortical engram for action patterns used in skilled reaching and the development of behavioral compensation following motor cortex lesions in the rat.* Neuropharmacology, 2000. **39**(5): p. 788-805.
60. Bao, C., et al., *The rat frontal orienting field dynamically encodes value for economic decisions under risk.* Nature Neuroscience, 2023. **26**(11): p. 1942-1952.
61. Rudebeck, P.H., et al., *Specialized Representations of Value in the Orbital and Ventrolateral Prefrontal Cortex: Desirability versus Availability of Outcomes.* Neuron, 2017. **95**(5): p. 1208-1220 e5.
62. Giovannucci, A., et al., *CaImAn an open source tool for scalable calcium imaging data analysis.* eLife, 2019. **8**: p. e38173.

TABLE 1

Across all Blocks in all Sessions for Rats with Lens Implants **γ = Probability Better Option**							
Formula	γ~[1 + Session + Schedule *Block * TrialNum * Area + (1 + Session + Block * TrialNum|RatID)]						
Coefficients	**β**	SE	tStat	DF	P	CIL	CIU
Intercept	1.4085	0.6099	2.3094	9433	0.0209	0.2129	2.6040
TrialNum	0.0559	0.0088	6.3735	9433	**<0.0001**	0.0387	0.0731
Schedule	0.1454	0.2598	0.5597	9433	0.5757	-0.3638	0.6546
Session	0.0578	0.0557	1.0376	9433	0.2995	-0.0514	0.1669
Area	1.6671	0.8182	2.0376	9433	**0.0416**	0.0633	3.2709
Block	-2.7860	0.4844	-5.7517	9433	**<0.0001**	-3.7355	-1.8365
TrialNum:Schedule	-0.0133	0.0031	-4.3179	9433	**<0.0001**	-0.0193	-0.0073
TrialNum:Area	0.0226	0.0118	1.9126	9433	0.0558	-0.0006	0.0458
Schedule:Area	-0.4912	0.3328	-1.4760	9433	0.1400	-1.1436	0.1612
TrialNum:Block	-0.0052	0.0031	-1.6777	9433	0.0934	-0.0113	0.0009
Schedule:Block	0.3826	0.2039	1.8761	9433	0.0607	-0.0171	0.7823
Area:Block	-2.0621	0.6598	-3.1253	9433	**0.0018**	-3.3555	-0.7687
TrialNum:Schedule:Area	-0.0078	0.0042	-1.8756	9433	0.0607	-0.0159	0.0004
TrialNum:Schedule:Block	0.0018	0.0011	1.6260	9433	0.1040	-0.0004	0.0039
TrialNum:Area:Block	0.0013	0.0042	0.3071	9433	0.7588	-0.0069	0.0094
Schedule:Area:Block	0.6375	0.2757	2.3122	9433	**0.0208**	0.0970	1.1780
TrialNum:Schedule:Area:Block	-0.0001	0.0015	-0.0730	9433	0.9418	-0.0030	0.0028

Alpha Level 0.05.

TABLE 2

Across all Blocks in all Sessions Comparing Lens Rats							
γ = Initiation Latency							
Formula	γ~[1+Session*Block*TrialNum+Area+(1+Session*Block*TrialNum|RatID)]						
Coefficients	**β**	SE	tStat	DF	P	CIL	CIU
(Intercept)	5.7688	1.5593	3.6996	9441	0.0002	2.7123	8.8254
TrialNum	-0.0450	0.0147	-3.0611	9441	**0.0022**	-0.0737	-0.0162
Session	-0.2227	0.2056	-1.0833	9441	0.2787	-0.6257	0.1803
Area	-0.4731	0.3832	-1.2344	9441	0.2171	-1.2242	0.2781
Block	0.0716	0.8186	0.0874	9441	0.9303	-1.5330	1.6762
TrialNum:Session	0.0053	0.0027	2.0071	9441	**0.0448**	0.0001	0.0105
TrialNum:Block	0.0114	0.0048	2.3661	9441	**0.0180**	0.0020	0.0209
Session:Block	-0.1536	0.1565	-0.9820	9441	0.3261	-0.4603	0.1530
TrialNum:Session:Block	-0.0010	0.0008	-1.2089	9441	0.2267	-0.0026	0.0006

Alpha Level 0.05

TABLE 3

Across all Blocks in all Sessions Comparing Lens Rats							
γ = Choice Latency							
Formula	γ~[1+Session*Block*TrialNum+Area+(1+Session*Block*TrialNum|RatID)]						
Coefficients	**β**	SE	tStat	DF	P	CIL	CIU
(Intercept)	2.0249	0.6468	3.1304	9441	0.0018	0.7569	3.2928
TrialNum	-0.0085	0.0065	-1.3061	9441	0.1916	-0.0213	0.0043
Session	0.0307	0.2050	0.1498	9441	0.8810	-0.3712	0.4326
Area	-0.5705	0.1600	-3.5666	9441	**0.0004**	-0.8840	-0.2569
Block	0.6944	0.4989	1.3920	9441	0.1640	-0.2835	1.6724
TrialNum:Session	-0.0006	0.0022	-0.2781	9441	0.7809	-0.0048	0.0036
TrialNum:Block	-0.0004	0.0032	-0.1219	9441	0.9030	-0.0066	0.0058
Session:Block	-0.1717	0.1449	-1.1843	9441	0.2363	-0.4558	0.1125
TrialNum:Session:Block	0.0008	0.0007	1.0717	9441	0.2839	-0.0006	0.0022

Alpha Level 0.05.

TABLE 4

Across all Blocks in all Sessions Comparing Lens Rats

γ = Reward Latency

Formula	γ~[1+Session*Block*TrialNum+Area+(1+Session*Block*TrialNum|RatID)]						
Coefficients	**β**	SE	tStat	DF	P	CIL	CIU
(Intercept)	1.5710	0.4575	3.4336	5809	0.0006	0.6740	2.4679
TrialNum	-0.0024	0.0032	-0.7300	5809	0.4654	-0.0087	0.0040
Session	-0.0524	0.0695	-0.7539	5809	0.4509	-0.1887	0.0839
Area	-0.3749	0.2199	-1.7047	5809	0.0883	-0.8060	0.0562
Block	0.2466	0.2591	0.9518	5809	0.3413	-0.2613	0.7545
TrialNum:Session	0.0002	0.0005	0.4166	5809	0.6770	-0.0008	0.0012
TrialNum:Block	-0.0002	0.0017	-0.0989	5809	0.9212	-0.0036	0.0032
Session:Block	-0.0540	0.0441	-1.2253	5809	0.2205	-0.1405	0.0324
TrialNum:Session:Block	0.0001	0.0003	0.2610	5809	0.7941	-0.0005	0.0007

Alpha Level 0.05

TABLE 5

Comparing Chosen Side Decoder Accuracy Across all Schedules in M2 and OFC **γ = Decoder Accuracy before Choice**							
Formula	γ~[1+Area*Schedule+Session+(1|RatID:Session)]						
Coefficients	**β**	SE	tStat	DF	P	CIL	CIU
(Intercept)	1.0210	0.0983	10.389	37	<0.0001	0.8219	1.2202
Area	-0.2312	0.0593	-3.9013	37	**0.0004**	-0.3513	-0.1111
Session	0.0268	0.0222	1.2109	37	0.2336	-0.0181	0.0718
Schedule	-0.0843	0.0633	-1.3307	37	0.1914	-0.2126	0.0440
Area:Schedule	0.0562	0.0274	2.0500	37	**0.0475**	0.0007	0.1118

Alpha Level 0.05**.**

TABLES 6 (Table 5 Post-Hoc)

Comparing Chosen Side Decoder Accuracy Across Schedules 1 ONLY in M2 and OFC **γ = Decoder Accuracy before Choice in Schedule 1**							
Formula	γ~[1+Area+(1|RatID:Session)]						
Coefficients	**β**	SE	tStat	DF	P	CIL	CIU
(Intercept)	0.9752	0.0661	14.755	12	<0.0001	0.8312	1.1192
Area	-0.1746	0.0401	-4.3533	12	**0.0009**	-0.2620	-0.0872

Comparing Chosen Side Decoder Accuracy Across Schedules 2 ONLY in M2 and OFC **γ = Decoder Accuracy before Choice in Schedule 2**							
Formula	γ~[1+Area+(1|RatID:Session)]						
Coefficients	**β**	SE	tStat	DF	P	CIL	CIU
(Intercept)	0.9503	0.0747	12.7138	12	<0.0001	0.787	1.113
Area	-0.1195	0.0454	-2.6330	12	**0.0219**	-0.218	-0.021

Comparing Chosen Side Decoder Accuracy Across Schedules 3 ONLY in M2 and OFC **γ = Decoder Accuracy before Choice in Schedule 3**							
Formula	γ~[1+Area+(1|RatID:Session)]						
Coefficients	**β**	SE	tStat	DF	P	CIL	CIU
(Intercept)	0.9140	0.0522	17.5113	12	<0.0001	0.800	1.028
Area	-0.0621	0.0317	-1.9613	12	0.0735	-0.131	0.007

Alpha Level 0.05.

788 **TABLE 7**

Comparing Trial Outcome Decoder Accuracy Across all Schedules in M2 and OFC **γ = Decoder Accuracy before Reward Cue**							
Formula	γ~[1+Area*Schedule+Session+(1|RatID:Session)]						
Coefficients	**β**	SE	tStat	DF	P	CIL	CIU
(Intercept)	0.8561	0.0976	8.7707	37	<0.0001	0.6583	1.0539
Area	-0.1378	0.0589	-2.3405	37	**0.0248**	-0.2571	-0.0185
Session	0.0300	0.0220	1.3612	37	0.1817	-0.0146	0.0746
Schedule	-0.1278	0.0629	-2.0321	37	**0.0494**	-0.2552	-0.0004
Area:Schedule	0.0482	0.0273	1.7686	37	0.0852	-0.0070	0.1034

789 Alpha Level 0.05.

790

791

TABLE 8

Comparing the Ratio of Side Selective Neurons Across all schedules in M2 and OFC **γ = Ratio of Side Selective Neurons**							
Formula	γ~[1+Area*Schedule+Session+(1|RatID)]						
Coefficients	**β**	SE	tStat	DF	P	CIL	CIU
(Intercept)	0.5512	0.0824	6.6895	37	<0.0001	0.3843	0.7182
Session	0.0208	0.0179	1.1569	37	0.2547	-0.0156	0.0571
Schedule	-0.0999	0.0512	-1.9501	37	0.0588	-0.2037	0.0039
Area	-0.2375	0.0497	-4.7775	37	**<0.0001**	-0.3383	-0.1368
Area:Schedule	0.0630	0.0222	2.8364	37	**0.0074**	0.0180	0.1079

Alpha Level 0.05

TABLE 9 (Table 8 Post-Hoc)

Comparing the Ratio of Side Selective Neurons Across all Schedules in M2 ONLY **γ = Ratio of Side Selective Neurons in M2**							
Formula	γ~[1+Schedule+(1|RatID)]						
Coefficients	**β**	SE	tStat	DF	P	CIL	CIU
(Intercept)	0.3033	0.0407	7.4487	16	<0.0001	0.2170	0.3896
Schedule	0.0046	0.0166	0.2758	16	0.7862	-0.0305	0.0397
Comparing the Ratio of Side Selective Neurons Across all Schedules in OFC ONLY **γ = Ratio of Side Selective Neurons in OFC**							
Formula	γ~[1+Schedule+(1|RatID)]						
Coefficients	**β**	SE	tStat	DF	P	CIL	CIU
(Intercept)	0.0658	0.0310	2.1207	22	<0.0001	0.0015	0.1301
Schedule	0.0675	0.0144	4.7031	22	**0.0001**	0.0378	0.0973

Alpha Level 0.05.

TABLE 10

Comparing the Ratio of Outcome Selective Neurons Across all schedules in M2 and OFC **γ = Ratio of Outcome Selective Neurons**							
Formula	γ~[1+Area*Schedule+Session+(1|RatID)]						
Coefficients	**β**	SE	tStat	DF	P	CIL	CIU
(Intercept)	0.3351	0.0897	3.7352	37	0.0006	0.1533	0.5168
Session	0.0181	0.0161	1.1285	37	0.2664	-0.0144	0.0507
Schedule	-0.0959	0.0459	-2.0875	37	**0.0438**	-0.1889	-0.0028
Area	-0.1020	0.0542	-1.8805	37	0.0679	-0.2119	0.0079
Area:Schedule	0.0447	0.0199	2.2443	37	**0.0309**	0.0043	0.0850

Alpha Level 0.05

TABLE 11 (Table 10 Post-Hoc)

Comparing the Ratio of Outcome Selective Neurons Across all Schedules in M2 ONLY **γ = Ratio of Outcome Selective Neurons in M2**							
Formula	γ~[1+Schedule+(1|RatID)]						
Coefficients	**β**	SE	tStat	DF	P	CIL	CIU
(Intercept)	0.2240	0.0415	5.4034	16	<0.0001	0.1361	0.3119
Schedule	-0.0149	0.0188	-0.7920	16	0.4399	-0.0548	0.0250
Comparing the Ratio of Outcome Selective Neurons Across all Schedules in OFC ONLY **γ = Ratio of Outcome Selective Neurons in OFC**							
Formula	γ~[1+Schedule+(1|RatID)]						
Coefficients	**β**	SE	tStat	DF	P	CIL	CIU
(Intercept)	0.1220	0.0358	3.4079	22	0.0025	0.0478	0.1963
Schedule	0.0297	0.0104	2.8584	22	**0.0091**	0.0082	0.0513

Alpha Level 0.05.

TABLE 12

Comparing the Ratio of Reward Selective Neurons Across all schedules in M2 and OFC **γ = Ratio of Reward Selective Neurons**							
Formula	γ~[1+Area*Schedule+Session+(1|RatID)]						
Coefficients	**β**	SE	tStat	DF	P	CIL	CIU
(Intercept)	0.7543	0.1819	4.1471	37	0.0002	0.3857	1.1228
Session	0.0080	0.0360	0.2223	37	0.8253	-0.0649	0.0809
Schedule	-0.1124	0.1028	-1.0940	37	0.2810	-0.3207	0.0958
Area	-0.2430	0.1099	-2.2120	37	**0.0332**	-0.4656	-0.0204
Area:Schedule	0.0909	0.0445	2.0408	37	**0.0484**	0.0007	0.1811

Alpha Level 0.05

TABLE 13 (Table 12 Post-Hoc)

Comparing the Ratio of Reward Selective Neurons Across all Schedules in M2 ONLY **γ = Ratio of Reward Selective Neurons in M2**							
Formula	γ~[1+Schedule+(1|RatID)]						
Coefficients	**β**	SE	tStat	DF	P	CIL	CIU
(Intercept)	0.5073	0.0390	12.9905	16	<0.0001	0.4245	0.5900
Schedule	-0.0056	0.0133	-0.4179	16	0.6816	-0.0337	0.0226
Comparing the Ratio of Reward Selective Neurons Across all Schedules in OFC ONLY **γ = Ratio of Reward Selective Neurons in OFC**							
Formula	γ~[1+Schedule+(1|RatID)]						
Coefficients	**β**	SE	tStat	DF	P	CIL	CIU
(Intercept)	0.2643	0.0906	2.9182	22	0.0080	0.0765	0.4521
Schedule	0.0853	0.0373	2.2886	22	**0.0321**	0.0080	0.1626

Alpha Level 0.05

TABLE 14

Decoder Accuracy modeled by Behavioral Measurements.
γ = Chosen Side Decoder Accuracy

Formula	γ~[1+Session+FlexibilityIndex+PerserverationIndex+InitiationLatency+ChoiceLatency+RewardLatency+WinStay+LoseShift+Area*(Session+FlexibilityIndex+PerserverationIndex+InitiationLatency+ChoiceLatency+RewardLatency+WinStay+LoseShift)+(1|RatID:Session)]						
Coefficients	**β**	SE	tStat	DF	P	CIL	CIU
(Intercept)	1.2994	0.4269	3.0436	25	0.0054	0.4201	2.1787
Initiation Latency	-0.0739	0.0653	-1.1326	25	0.2681	-0.2083	0.0605
Choice Latency	0.0264	0.1127	0.2344	25	0.8166	-0.2057	0.2586
Reward Latency	-0.0873	0.0783	-1.1152	25	0.2754	-0.2484	0.0739
WinStay	-1.5011	0.8803	-1.7052	25	0.1006	-3.3140	0.3119
Area	-0.5611	0.2587	-2.1691	25	**0.0398**	-1.0939	-0.0283
LoseShift	-2.2113	1.4948	-1.4793	25	0.1515	-5.2899	0.8673
Flexibility Index	1.1537	0.8096	1.4250	25	0.1665	-0.5137	2.8211
Perseveration Index	3.9990	1.6714	2.3926	25	**0.0246**	0.5566	7.4413
Session	0.0035	0.0099	0.3565	25	0.7244	-0.0168	0.0238
Area:InitiationLatency	0.0608	0.0407	1.4962	25	0.1471	-0.0229	0.1446
Area:ChoiceLatency	-0.0599	0.0841	-0.7127	25	0.4826	-0.2331	0.1132
Area:RewardLatency	0.0242	0.0438	0.5542	25	0.5844	-0.0659	0.1144
Area:Win Stay	1.3807	0.5670	2.4352	25	**0.0224**	0.2130	2.5485
Area:Lose Shift	2.1181	0.9107	2.3258	25	**0.0284**	0.2425	3.9937
Area:Flexibility Index	-0.7755	0.5260	-1.4743	25	0.1529	-1.8589	0.3078
Area:Perseveration Index	-3.9170	1.0290	-3.8066	25	**0.0008**	-6.0363	-1.7978

Alpha Level 0.05

TABLE 15 (Table 14 Post-Hoc)

Post-Hoc Statistics on Area Interaction with M2 Lens Rats only **γ = Chosen Side Decoder Accuracy in M2 Rats**							
Formula	γ~[1+PerseverationIndex+WinStay+LoseShift+(1|RatID:Session)]						
Coefficients	**β**	SE	tStat	DF	P	CIL	CIU
(Intercept)	0.9846	0.1674	5.8818	14	<0.0001	0.6255	1.3436
Win Stay	-0.0131	0.1558	-0.0839	14	0.9343	-0.3472	0.3210
Lose Shift	-0.6778	0.5746	-1.1796	14	0.2578	-1.9102	0.5546
Perseveration Index	-1.0741	0.7841	-1.3699	14	0.1923	-2.7559	0.6076

Post-Hoc Statistics on Area Interaction with OFC Lens Rats only **γ = Chosen Side Decoder Accuracy in OFC Rats**							
Formula	γ~[1+PerseverationIndex+WinStay+LoseShift+(1|RatID:Session)]						
Coefficients	**β**	SE	tStat	DF	P	CIL	CIU
(Intercept)	0.2041	0.1828	1.1167	20	0.2774	-0.1771	0.5853
Win Stay	0.8435	0.2010	4.1975	20	**0.0004**	0.4243	1.2627
Lose Shift	1.4664	0.5304	2.7648	20	**0.0120**	0.3600	2.5729
Perseveration Index	-4.1286	0.6312	-6.5405	20	**<0.0001**	-5.4453	-2.8118

Alpha Level 0.05

TABLE 16

Decoder Accuracy modeled by Behavioral Measurements.
γ = **Trial Outcome Decoder Accuracy**

Formula	γ~[1+Session+FlexibilityIndex+PerserverationIndex+InitiationLatency+ChoiceLatency+RewardLatency+WinStay+LoseShift+Area*(Session+FlexibilityIndex+PerserverationIndex+InitiationLatency+ChoiceLatency+RewardLatency+WinStay+LoseShift)+(1|RatID:Session)]						
Coefficients	**β**	SE	tStat	DF	P	CIL	CIU
Intercept	1.4433	0.4581	3.1505	25	0.0042	0.4998	2.3868
Initiation Latency	-0.1490	0.0700	-2.1278	25	**0.0434**	-0.2932	-0.0048
Choice Latency	0.0677	0.1210	0.5595	25	0.5808	-0.1814	0.3168
Reward Latency	0.1892	0.0840	2.2530	25	**0.0333**	0.0162	0.3621
WinStay	-2.0423	0.9446	-2.1622	25	**0.0404**	-3.9877	-0.0970
Area	-0.7024	0.2776	-2.5304	25	**0.0181**	-1.2741	-0.1307
LoseShift	-2.7002	1.6040	-1.6835	25	0.1047	-6.0037	0.6032
Flexibility Index	0.8666	0.8687	0.9976	25	0.3281	-0.9226	2.6557
Perseveration Index	3.7763	1.7935	2.1056	25	**0.0455**	0.0826	7.4700
Session	0.0087	0.0106	0.8186	25	0.4207	-0.0131	0.0305
Area:InitiationLatency	0.0946	0.0436	2.1676	25	**0.0399**	0.0047	0.1845
Area:ChoiceLatency	-0.0641	0.0902	-0.7109	25	0.4837	-0.2499	0.1217
Area:RewardLatency	-0.0971	0.0469	-2.0688	25	**0.0491**	-0.1938	-0.0004
Area:WinStay	1.5174	0.6084	2.4940	25	**0.0196**	0.2643	2.7704
Area:LoseShift	2.3028	0.9772	2.3565	25	**0.0266**	0.2902	4.3154
Area:Flexibility Index	-0.6076	0.5644	-1.0765	25	0.2920	-1.7701	0.5549
Area:Perseveration Index	-2.4325	1.1041	-2.2031	25	**0.0370**	-4.7065	-0.1585

Alpha Level 0.05

TABLE 17 (Table 16 Post-Hoc)

Post-Hoc Statistics on Area Interaction with M2 Lens Rats only **γ = Trial Outcome Decoder Accuracy in M2 Rats**							
Formula	γ~[1+PerseverationIndex+InitiationLatency+RewardLatency+Win Stay+LoseShift+(1|RatID:Session)]						
Coefficients	**β**	SE	tStat	DF	P	CIL	CIU
(Intercept)	0.8398	0.1998	4.2042	12	0.0012	0.4046	1.2750
Initiation Latency	-0.0678	0.0281	-2.4183	12	**0.0324**	-0.1290	-0.0067
Reward Latency	0.0835	0.0398	2.0961	12	0.0579	-0.0033	0.1703
Win Stay	-0.2921	0.2255	-1.2951	12	0.2197	-0.7834	0.1993
Lose Shift	-0.1878	0.6896	-0.2723	12	0.7901	-1.6903	1.3148
Perseveration Index	0.9463	0.8409	1.1254	12	0.2824	-0.8858	2.7785

Post-Hoc Statistics on Area Interaction with OFC Lens Rats only **γ = Trial Outcome Decoder Accuracy in OFC Rats**							
Formula	γ~[1+PerseverationIndex+InitiationLatency+RewardLatency+Win Stay+LoseShift+(1|RatID:Session)]						
Coefficients	**β**	SE	tStat	DF	P	CIL	CIU
(Intercept)	0.0749	0.1868	0.4007	18	0.6934	-0.3176	0.4674
Initiation Latency	0.0193	0.0151	1.2789	18	0.2172	-0.0124	0.0509
Reward Latency	-0.0069	0.0236	-0.2919	18	0.7737	-0.0564	0.0426
Win Stay	0.6517	0.2268	2.8730	18	**0.0101**	0.1751	1.1283
Lose Shift	1.5504	0.5505	2.8161	18	**0.0114**	0.3937	2.7070
Perseveration Index	-1.5430	0.6310	-2.4452	18	**0.0249**	-2.8687	-0.2172

Alpha Level 0.05

TABLE 18

Across all Blocks in all Sessions for Rats with DREADDs in OFC γ = **Probability Better Option**							
Formula	γ ~ [1 + Drug*Schedule*Order + TrialNum*Block + Sex + (1 + TrialNum*Block | RatID)]						
Coefficients	**β**	SE	tStat	DF	P	CIL	CIU
Intercept	3.4514	0.3179	10.8558	20238	<0.0001	2.8282	4.0746
TrialNum	0.0364	0.0031	11.8630	20238	**<0.0001**	0.0303	0.0424
Schedule	-0.1897	0.0377	-5.0383	20238	**<0.0001**	-0.2635	-0.1159
Order	1.2519	0.1697	7.3779	20238	**<0.0001**	0.9193	1.5845
Sex	-0.0729	0.0726	-1.0052	20238	0.3148	-0.2152	0.0693
Drug	-0.2831	0.1204	2.3502	20238	**0.0188**	0.0470	0.5192
Block	-3.0267	0.2796	-10.823	20238	**<0.0001**	-3.5748	-2.4786
Schedule:Order	-0.4388	0.0967	-4.5357	20238	**<0.0001**	-0.6284	-0.2492
Schedule:Drug	-0.0222	0.0545	-0.4071	20238	0.6839	-0.1291	0.0847
Order:Drug	-0.3706	0.2443	-1.5169	20238	0.1293	-0.8495	0.1083
TrialNum:Block	0.0002	0.0009	0.1891	20238	0.8500	-0.0015	0.0019
Schedule:Order :Drug	0.1861	0.1397	1.3321	20238	0.1829	-0.0877	0.4599

Alpha Level 0.05

848

849 **TABLE 19**

Across all Blocks in all Sessions for Rats with DREADDs in M2 γ = **Probability Better Option**							
Formula	γ ~ [1 + Drug*Schedule*Order + TrialNum*Block + Sex + (1 + TrialNum*Block | RatID)]						
Coefficients	**β**	SE	tStat	DF	P	CIL	CIU
Intercept	2.2371	0.3472	6.4436	20238	<0.0001	1.5566	2.9175
TrialNum	0.0200	0.0047	4.2983	20238	**<0.0001**	0.0109	0.0292
Schedule	0.0702	0.0346	2.0301	20238	**0.0424**	0.0024	0.1381
Order	0.7681	0.1371	5.6007	20238	**0.0000**	0.4993	1.0368
Sex	0.2504	0.1193	2.0995	20238	**0.0358**	0.0166	0.4842
Drug	-0.4698	0.1066	4.4067	20238	**<0.0001**	0.2609	0.6788
Block	-2.4059	0.2808	-8.5687	20238	**<0.0001**	-2.9563	-1.8556
Schedule:Order	-0.3030	0.0799	-3.7922	20238	**0.0001**	-0.4596	-0.1464
Schedule:Drug	-0.1866	0.0492	-3.7900	20238	**0.0002**	-0.2832	-0.0901
Order:Drug	-0.4036	0.1956	-2.0637	20238	**0.0391**	-0.7869	-0.0203
TrialNum:Block	0.0027	0.0012	2.2015	20238	**0.0277**	0.0003	0.0052
Schedule:Order :Drug	0.1914	0.1137	1.6829	20238	0.0924	-0.0315	0.4142

850 Alpha Level 0.05

851

852

853

854

855

856

857

858

TABLE 20 (Table 19 Post-Hoc)

Post-Hoc Statistics on Schedule by Drug Interaction with Schedule 1 collapsed, M2 Rats γ = **Probability Better Option**							
Formula	γ ~ [1+Drug+Sex+Block*TrialNum+(1+Block*TrialNum|Rat)]						
Coefficients	**β**	SE	tStat	DF	P	CIL	CIU
(Intercept)	2.3493	0.3596	6.5333	8094	<0.0001	1.6444	3.0542
TrialNum	0.0212	0.0050	4.2491	8094	**<0.0001**	0.0114	0.0310
Sex	0.4271	0.1365	3.1299	8094	**0.0018**	0.1596	0.6947
Drug	-0.2018	0.0505	3.9978	8094	**0.0001**	0.1028	0.3007
Block	-2.4932	0.2741	-9.0943	8094	**<0.0001**	-3.0306	-1.9558
TrialNum:Block	0.0030	0.0015	1.9742	8094	**0.0484**	0.0000	0.0061

Post-Hoc Statistics on Schedule by Drug Interaction with Schedule 2 collapsed, M2 Rats γ = **Probability Better Option**							
Formula	γ ~ [1+Drug+Sex+Block*TrialNum+(1+Block*TrialNum|Rat)]						
Coefficients	**β**	SE	tStat	DF	P	CIL	CIU
(Intercept)	2.4211	0.3567	6.7876	8094	<0.0001	1.7219	3.1203
TrialNum	0.0264	0.0064	4.1355	8094	**<0.0001**	0.0139	0.0390
Sex	0.2689	0.1034	2.6021	8094	**0.0093**	0.0663	0.4715
Drug	-0.0476	0.0507	0.9380	8094	0.3483	-0.0518	0.1470
Block	-2.4086	0.3349	-7.1911	8094	**<0.0001**	-3.0651	-1.7520
TrialNum:Block	0.0008	0.0016	0.4725	8094	0.6366	-0.0024	0.0040

Post-Hoc Statistics on Schedule by Drug Interaction with Schedule 3 collapsed, M2 Rats γ = **Probability Better Option**							
Formula	γ ~ [1+Drug+Sex+Block*TrialNum+(1+Block*TrialNum|Rat)]						
Coefficients	**β**	SE	tStat	DF	P	CIL	CIU
(Intercept)	2.6601	0.5251	5.0659	4044	<0.0001	1.6306	3.6896
TrialNum	0.0071	0.0056	1.2606	4044	0.2075	-0.0039	0.0180
Sex	0.4522	0.1762	2.5666	4044	**0.0103**	0.1068	0.7975
Drug	0.0491	0.0684	-0.7179	4044	0.4728	-0.1832	0.0850
Block	-2.3052	0.3974	-5.8000	4044	**<0.0001**	-3.0844	-1.5260
TrialNum:Block	0.0057	0.0021	2.7799	4044	**0.0055**	0.0017	0.0098

Alpha Level 0.05

TABLE 21 (Table 19 Post-Hoc)

Post-Hoc Statistics on Order by Drug Interaction with Ascending collapsed, M2 Rats γ = **Probability Better Option**							
Formula	γ ~ [1+Drug+Sex+Block*TrialNum+(1+Block*TrialNum|Rat)]						
Coefficients	**β**	SE	tStat	DF	P	CIL	CIU
(Intercept)	2.6389	0.3007	8.7758	12144	<0.0001	2.0495	3.2284
TrialNum	0.0180	0.0049	3.6885	12144	**0.0002**	0.0084	0.0276
Sex	0.0654	0.1015	0.6447	12144	0.5192	-0.1335	0.2644
Drug	-0.0950	0.0400	2.3744	12144	**0.0176**	0.0166	0.1735
Block	-2.5241	0.2593	-9.7345	12144	**<0.0001**	-3.0324	-2.0158
TrialNum:Block	0.0037	0.0013	2.7929	12144	**0.0052**	0.0011	0.0063

Post-Hoc Statistics on Order by Drug Interaction with Descending collapsed, M2 Rats γ = **Probability Better Option**							
Formula	γ ~ [1+Drug+Sex+Block*TrialNum+(1+Block*TrialNum|Rat)]						
Coefficients	**β**	SE	tStat	DF	P	CIL	CIU
(Intercept)	2.2890	0.4609	4.9665	8094	<0.0001	1.3856	3.1925
TrialNum	0.0243	0.0051	4.7432	8094	**<0.0001**	0.0143	0.0344
Sex	0.5643	0.1814	3.1111	8094	**0.0019**	0.2088	0.9199
Drug	-0.0757	0.0520	1.4559	8094	0.1455	-0.0262	0.1777
Block	-2.2855	0.3692	-6.1910	8094	**<0.0001**	-3.0091	-1.5618
TrialNum:Block	0.0012	0.0014	0.8352	8094	0.4036	-0.0016	0.0039

Alpha Level: 0.05

866 **TABLE 22**

Across all Sessions for Rats with DREADDs in OFC γ = **Win-Stay**							
Formula	γ ~ [1 + Drug*Schedule*Order + Sex + (1 | Rat)](1 | RatID)]						
Coefficients	**β**	SE	tStat	DF	P	CIL	CIU
Intercept	0.6894	0.0293	23.5256	81	<0.0001	0.6311	0.7477
Schedule	-0.0548	0.0112	-4.8942	81	**<0.0001**	-0.0771	-0.0325
Order	0.2558	0.0429	5.9638	81	**<0.0001**	0.1705	0.3411
Sex	-0.0329	0.0232	-1.4209	81	0.1592	-0.0791	0.0132
Drug	-0.0782	0.0342	2.2852	81	**0.0249**	0.0101	0.1463
Schedule:Order	-0.0923	0.0250	-3.6874	81	**0.0004**	-0.1422	-0.0425
Schedule:Drug	-0.0138	0.0158	-0.8730	81	0.3853	-0.0453	0.0177
Order:Drug	-0.0826	0.0607	-1.3623	81	0.1769	-0.2033	0.0381
Schedule:Order:Drug	0.0341	0.0354	0.9621	81	0.3389	-0.0364	0.1045

867 Alpha Level 0.05

868

869 **TABLE 23**

Across all Sessions for Rats with DREADDs in M2 γ = **Win-Stay**							
Formula	γ ~ [1 + Drug*Schedule*Order + Sex + (1 | Rat)]						
Coefficients	**β**	SE	tStat	DF	P	CIL	CIU
Intercept	0.5246	0.0557	9.4118	81	<0.0001	0.4137	0.6355
Schedule	-0.0015	0.0190	-0.0781	81	0.9379	-0.0392	0.0363
Order	0.1949	0.0726	2.6828	81	**0.0088**	0.0504	0.3394
Sex	-0.1342	0.0520	-2.5838	81	**0.0116**	-0.2376	-0.0309
Drug	-0.0863	0.0580	1.4884	81	0.1405	-0.0291	0.2016
Schedule:Order	-0.0790	0.0424	-1.8627	81	0.0661	-0.1634	0.0054
Schedule:Drug	-0.0328	0.0268	-1.2241	81	0.2245	-0.0862	0.0205
Order:Drug	-0.0443	0.1027	-0.4310	81	0.6676	-0.2487	0.1601
Schedule:Order:Drug	0.0185	0.0600	0.3087	81	0.7583	-0.1008	0.1379

870 Alpha Level 0.05

871

872

873

874

875

876

877

878

879 **TABLE 24**

Across all Sessions for Rats with DREADDs in OFC γ = **Lose-Shift**							
Formula	γ ~ [1 + Drug*Schedule*Order + Sex + (1 | Rat)]						
Coefficients	**β**	SE	tStat	DF	P	CIL	CIU
Intercept	0.1143	0.0161	7.0819	81	<0.0001	0.0822	0.1464
Schedule	0.0272	0.0056	4.8427	81	**<0.0001**	0.0160	0.0383
Order	-0.0825	0.0215	-3.8395	81	**0.0002**	-0.1252	-0.0397
Sex	0.0014	0.0147	0.0968	81	0.9231	-0.0278	0.0306
Drug	0.0184	0.0171	-1.0760	81	0.2851	-0.0525	0.0157
Schedule:Order	0.0291	0.0125	2.3232	81	**0.0227**	0.0042	0.0541
Schedule:Drug	-0.0010	0.0079	-0.1245	81	0.9012	-0.0168	0.0148
Order:Drug	0.0189	0.0304	0.6232	81	0.5349	-0.0415	0.0794
Schedule:Order:Drug	-0.0074	0.0177	-0.4177	81	0.6773	-0.0427	0.0279

880 Alpha Level 0.05

881

882 **TABLE 25**

Across all Sessions for Rats with DREADDs in M2 γ = **Lose-Shift**							
Formula	γ ~ [1 + Drug*Schedule*Order + Sex + (1 | Rat)]						
Coefficients	**β**	SE	tStat	DF	P	CIL	CIU
Intercept	0.1584	0.0225	7.0291	81	<0.0001	0.1135	0.2032
Schedule	0.0057	0.0080	0.7105	81	0.4794	-0.0102	0.0216
Order	-0.0514	0.0306	-1.6777	81	0.0973	-0.1123	0.0095
Sex	0.0349	0.0200	1.7466	81	0.0845	-0.0049	0.0747
Drug	-0.0026	0.0244	-0.1079	81	0.9144	-0.0512	0.0460
Schedule:Order	0.0225	0.0179	1.2571	81	0.2123	-0.0131	0.0580
Schedule:Drug	-0.0025	0.0113	-0.2184	81	0.8276	-0.0250	0.0200
Order:Drug	-0.0122	0.0433	-0.2814	81	0.7791	-0.0983	0.0740
Schedule:Order:Drug	-0.0514	0.0306	-1.6777	81	0.0973	-0.1123	0.0095

883 Alpha Level 0.05

884

885

886

TABLE 26

Across all Sessions for Rats with DREADDs in M2 γ = **Choice Latency**							
Formula	γ ~ [1 + Drug*Schedule*Order + Sex + (1 | Rat)]						
Coefficients	**β**	SE	tStat	DF	P	CIL	CIU
Intercept	0.5028	0.2232	2.2530	81	0.0270	0.0588	0.9468
Schedule	0.1222	0.0970	1.2599	81	0.2113	-0.0708	0.3151
Order	0.0091	0.3713	0.0246	81	0.9804	-0.7297	0.7480
Sex	0.3677	0.1185	3.1020	81	**0.0026**	0.1319	0.6036
Drug	-0.1114	0.2962	-0.3760	81	0.7079	-0.7008	0.4780
Schedule:Order	0.0183	0.2168	0.0843	81	0.9330	-0.4131	0.4497
Schedule:Drug	0.0592	0.1371	0.4315	81	0.6673	-0.2137	0.3320
Order:Drug	0.1751	0.5251	0.3335	81	0.7396	-0.8697	1.2200
Schedule:Order:Drug	-0.0578	0.3066	-0.1886	81	0.8509	-0.6679	0.5522

Alpha Level 0.05

TABLE 27

Across all Sessions for Rats with DREADDs in OFC γ = **Choice Latency**							
Formula	γ ~ [1 + Drug*Schedule*Order + Sex + (1 | Rat)]						
Coefficients	**β**	SE	tStat	DF	P	CIL	CIU
Intercept	1.2705	0.2036	6.2401	81	<0.0001	0.8654	1.6756
Schedule	-0.0897	0.0616	-1.4576	81	0.1488	-0.2122	0.0327
Order	-0.6209	0.2357	-2.6341	81	**0.0101**	-1.0900	-0.1519
Sex	0.0135	0.2101	0.0643	81	0.9489	-0.4046	0.4316
Drug	-0.3819	0.1880	-2.0306	81	**0.0456**	-0.7560	-0.0077
Schedule:Order	0.1862	0.1376	1.3526	81	0.1799	-0.0877	0.4600
Schedule:Drug	0.1301	0.0870	1.4940	81	0.1390	-0.0431	0.3033
Order:Drug	0.4106	0.3334	1.2317	81	0.2216	-0.2527	1.0739
Schedule:Order:Drug	-0.2023	0.1946	-1.0392	81	0.3018	-0.5896	0.1850

Alpha Level 0.05